AD-A038 496 FRANKFORD ARSENAL PHILADELPHIA PA F/G 19/1
COMPUTER-AIDED MODELING OF ARTILLERY SHELL AND CARTRIDGE CASE D--ETC(U)
APR 76 P F GORDON, F M LEE
UNCLASSIFIED FA-TR-76020 NL

1 OF 2
AD A038496

END CONT.
DATE FILMED 5-77

AD

FA-TR-76020

COMPUTER-AIDED MODELING OF ARTILLERY SHELL AND CARTRIDGE CASE DRAWING

By

P.F. Gordon
F.M. Lee

April 1976

Approved for public release; distribution unlimited.

Pitman-Dunn Laboratory

U.S. ARMY ARMAMENT COMMAND
FRANKFORD ARSENAL
PHILADELPHIA, PENNSYLVANIA 19137

DISPOSITION INSTRUCTIONS

Destroy this report when no longer needed. Do not return it to the originator.

The findings in this report are not to be construed as an official Department of the Army position unless so designated by other authorized documents.

TABLE OF CONTENTS

LIST OF ILLUSTRATIONS

LIST OF TABLES

UNCLASSIFIED

SECURITY CLASSIFICATION OF THIS PAGE (When Data Entered)

REPORT DOCUMENTATION PAGE

READ INSTRUCTIONS BEFORE COMPLETING FORM

1. REPORT NUMBER: FA-TR-76020	2. GOVT ACCESSION NO.
3. RECIPIENT'S CATALOG NUMBER	
4. TITLE (and Subtitle): COMPUTER-AIDED MODELING OF ARTILLERY SHELL AND CARTRIDGE CASE	5. TYPE OF REPORT & PERIOD COVERED: Technical Research Report,
	6. PERFORMING ORG. REPORT NUMBER
7. AUTHOR(s): Paul F. Gordon Fee Men Lee	8. CONTRACT OR GRANT NUMBER(s)
9. PERFORMING ORGANIZATION NAME AND ADDRESS FRANKFORD ARSENAL Attn: SARFA-PDM-E Philadelphia, PA 19137	10. PROGRAM ELEMENT, PROJECT, TASK AREA & WORK UNIT NUMBERS AMCMS CODE: 4932056550 DA PROJECT: 5736550
11. CONTROLLING OFFICE NAME AND ADDRESS FRANKFORD ARSENAL Philadelphia, PA 19137	12. REPORT DATE: April 1976 13. NUMBER OF PAGES: 90
14. MONITORING AGENCY NAME & ADDRESS (if different from Controlling Office)	15. SECURITY CLASS. (of this report): UNCLASSIFIED 15a. DECLASSIFICATION/DOWNGRADING SCHEDULE: N/A

16. DISTRIBUTION STATEMENT (of this Report)

Approved for public release; distribution unlimited.

17. DISTRIBUTION STATEMENT (of the abstract entered in Block 20, if different from Report)

18. SUPPLEMENTARY NOTES

The authors would like to express appreciation to the staff of the Manufacturing Technology Directorate for their careful review of this report. Of particular importance is the contribution of Mssrs. R. Meinert and M. Grum in pointing out the role of plastic instability in shell drawing.

19. KEY WORDS (Continue on reverse side if necessary and identify by block number)

Optimal die	Billet	C.A.D.
Perturbation	Mandrel	C.A.M.
Computer simulation	Temperature distribution	Cartridge case
Tapered die	Friction	
Curved die	Upper bound	

20. ABSTRACT (Continue on reverse side if necessary and identify by block number)

Mathematical models which simulate the drawing of artillery shell with a moving mandrel were developed and computerized. The models are applicable to conventional, tapered dies; or to curved, streamlined die profiles. Studies on the effects of important process variables (temperature, friction, punch speed, material) on the drawability of a 105 mm shell were performed, and die design charts prepared. A new optimal die profile, which requires less energy from the forming press, was designed. It was

DD FORM 1 JAN 73 1473 EDITION OF 1 NOV 65 IS OBSOLETE

UNCLASSIFIED

SECURITY CLASSIFICATION OF THIS PAGE (When Data Entered)

142 720

20. ABSTRACT (Cont)

also established that a maximum areal reduction of about 40% was an upper bound for cold drawing. Limitations of the simulation procedure were identified. Recommendations for corroborative experimental work and for future modeling efforts were made.

INTRODUCTION

The objective of the MM&T Project 6550 was to perform engineering studies and surveys of industry in order to assure that the methods of shell production in modernized Army plants were consistent with the latest state of art in manufacturing technology. This task dealt with the modeling and computer simulation of the drawing operation in shell manufacture. Specifically, for shell drawing, the task objectives were: (a) to provide analytical models describing the forming of artillery shell and cartridge cases, and (b) to optimize the modeled process. The work performed under this task is presented in this report.

In current shell manufacturing practice, the shell is formed to have an almost finished internal cavity surface with the finish machining largely relegated to the outside surface of the piece. Nosing then occurs after rough machining is completed. There are three basic methods of introducing a shell cavity into the slug or billet: (1) Hot piercing followed by hot drawing, (2) Cold extrusion and drawing and (3) Hot cupping followed by cold drawing. In each of these methods of initial shell forming, the drawing process, whether hot or cold, is the essential basic step of the several forming operations involved. Consequently, due to its basic technological importance, drawing was selected as the first operation to be modeled.

This study was also undertaken because of a lack of data in manufacturing using mechanical presses. Projected shell lines will use mechanical presses, or a combination of mechanical and hydraulic presses, rather than the conventional purely hydraulic systems. Data on draw feasibility and process design with a mechanical press for artillery shell is very limited. This sparsity of data on processing with mechanical presses at elevated speeds presents design, planning and commonality problems for both current and projected production lines. The models of the drawing process, as documented in this report, can provide reliable guidelines for process design with mechanical press systems. This study on shell drawing supports all current and projected 105mm and 155mm lines. The computer programs generated under this task are, however, general enough to support any size shell.

The objectives of this task were met by a combination of in-house and contractural effort with Battelle-Columbus Laboratories. Battelle[1] developed the math models associated with the curved die profiles, optimization and a portion of the heat transfer work. These efforts have been thoroughly documented in a report[1] which shows the details of the models and the computer programs. Part of the Frankford effort consisted of developing math models associated with failure during drawing, heat transfer and conventional tapered die profiles. The present report unifies these two development efforts by presenting results drawn from both sources. All models generated under this task have been made functional on the CDC 6000 series computers at

---

(1) References are given at the end of this report.

Picatinny Arsenal via remote entry from Frankford Arsenal. All the numerical results presented in this report were generated at Frankford Arsenal.

As a result of this study a new curved die configuration was designed which requires a minimum energy expenditure from the press for any specified reduction, either hot or cold. The new die should require 10-15% less energy than a conventional straight profile ring performing the same reduction. The effects of processing conditions such as temperature, punch speed, friction and reduction for the new configuration were studied in order to present criteria which avoid punch through failure. Concrete example designs were performed for the cold drawing of a 105mm shell forging using a variety of current steels. It was found that 40-42% reduction in a single pass, cold operation is the upper limit of draw feasibility for a 105mm shell. Treated also in this report were conventional tapered dies. Design curves covering a wide range of processing variables including failure were prepared. In general, for both curved and tapered dies, it was established that the temperature in hot forming plays a key role in limiting potential operating press speed.

The remainder of this report is organized as follows: specific data dealing with optimal curved dies and conventional tapered dies are presented in the Simulation Results section. Interpretation of the data and conclusions are presented in the Summary and Discussion. The mathematical models used have been placed separately in Appendix A and B, rather than in the text proper. It is not necessary for users of the data in this report to refer to these Appendicies. Previous models, a literature survey and assessments of the state of the art in simulation have, because of their length, been placed in Appendix A.

SIMULATION RESULTS

I OPTIMAL CURVED DIES

On the basis of the Battelle[1] study, it was found that curved die profiles could be designed which were optimal. Optimal in this context has the following meaning: for a given reduction, material and lubrication (friction), condition there is a curved die profile which, when compared to a conventional, tapered profile is superior in that:

a. Less energy is required to form,

b. The flow of metal is such that the strains at the exit are uniform through the shell wall.

The first factor implies a potential cost reduction by conserving press power. The second factor implies a reduction in liklihood of material failure or "punch through" by the mandrel. Experimental studies indicate that the product, due to the radial homogeneity of the strains developed, will also show improved metallurgical properties.

This report extends the above findings by considering the influence of various processing variables and materials on the design of optimal, curved dies. The computer program CDVEL was used. An extended discussion of the mathematical model in CDVEL is to be found in Reference 1, and is also summarized in section II. A of Appendix A of this report.

Figure 1 shows the problem under consideration. A shell is being drawn through a die (cross hatched) whose inner surface is doubly curved by two circular arcs of radii R_1 and R_2. A punch of radius r_o is moving the material from left to right with an entry speed V_o and an exit speed of Ve. The basic problem is to determine the profile (i. e., R_1 and R_2) in the optimal manner described above.

The results to be presented are, as in Reference 1, for the 40% reduction of a 105mm shell in a single pass with an untapered punch. The product thus has a constant wall thickness. The baseline conditions for cold and hot drawing used here are in Table 1. Departures from these values are indicated in the text as necessary.

The effect of using various commonly used shell steels on optimal shape in a cold 40% draw are shown in Figure 2. This graph represents the actual contour (in mm) of the optimal curved die for each steel. The radial coordinate (R(z) of Figure 1) is plotted as a function of the axial coordinate (z of Figure 1). The actual data points, which are automatically printed by the computer, are given in Table 2. (Except for two steels, 52100 and 1095, the material properties are taken at 20° C - cold. The 52100 and 1095 runs were made at 750° C, the lowest temperature for which material properties were available. As can be immediately seen, the optimal die profile is essentially the same for each steel except for the 4337). Thus, the important conclusion: For cold and moderately warm drawing at moderate speeds the optimal die profile is essentially the same for all steels.

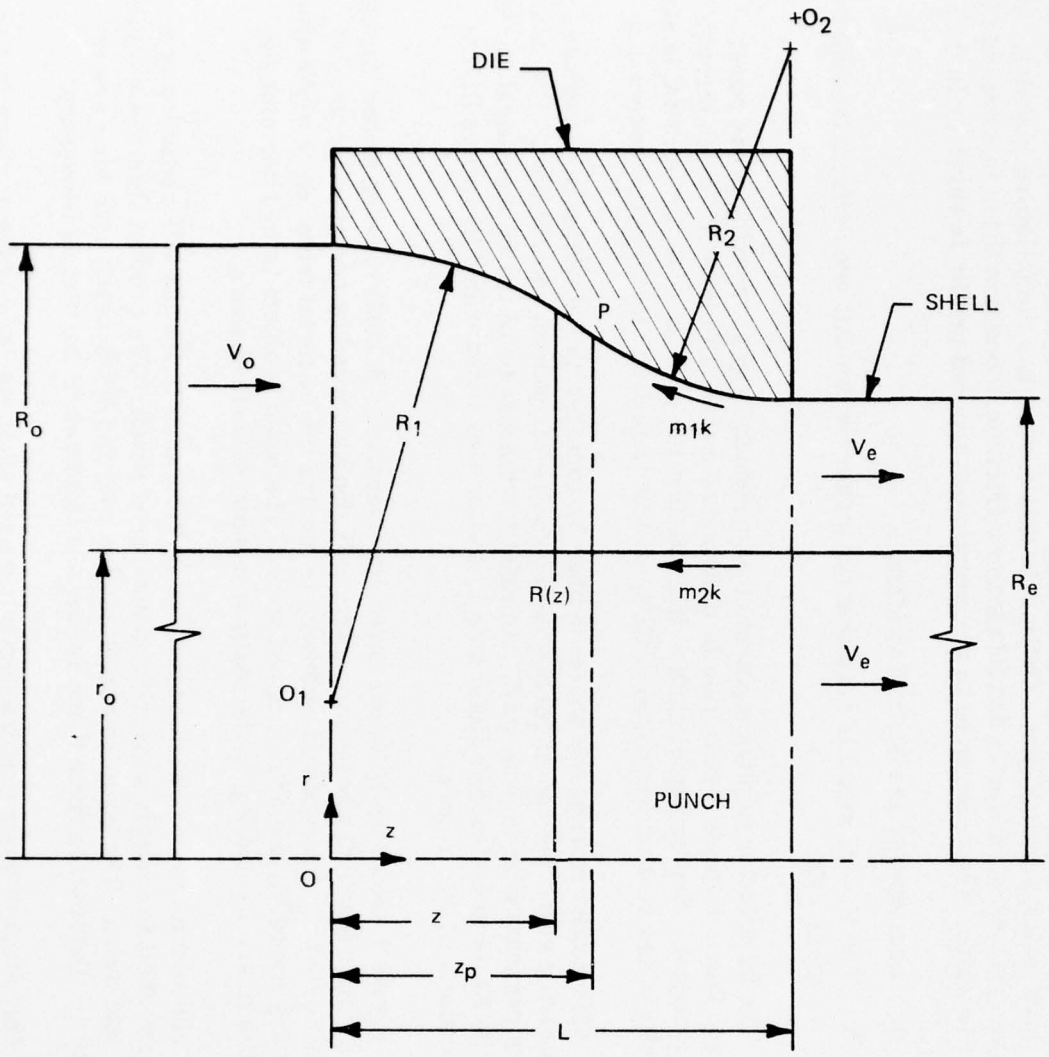

Figure 1. Schematic Diagram of Shell Drawing Through A Double Curvature Die

Table 1. Conditions Used for Theoretical Determination Of The Die Shape And For The Prediction Of Process Variables

Billet Material	=	AISI 1045 Steel(*)
Billet Outside Diameter	=	140 mm
Billet Inside Diameter	=	86 mm
Punch Diameter	=	86 mm
Reduction in Area of Cross Section	=	40 Percent
Punch Speed	=	100 mm/sec (cold)
	=	1000 mm/sec (hot)
Friction Shear Factor m_1 (die/shell)	=	0.1 (cold)
	=	0.25 (hot)
Friction Shear Factor m_2 (die/mandrel)	=	0.2 (cold)
	=	0.35 (hot)
Billet Temperature	=	20° C (cold)
	=	1000° C (hot)

(*)The flow stress data for this material were obtained from Reference 29.

Table 3 shows the drawing data for the above steels. Examining the specific draw stress, which represents failure by punch through if it exceeds unity (Appendix A): (the 1095 and 52100 steels are totally inadequate at 750° C; with 40% reduction failure will certainly occur. The same steels in the cold condition may be adequate at a 40% reduction.) The 4337 steel is marginal for failure; the remaining steels should not experience failure.

The energy rates for the failed steels are much lower than for the safe materials. Similar commentary applies to the drawing load and the punch load. These facts are explained by the fact that the yield strength has been degraded in the two metals which failed. Thus a much lower energy and load system resulted. Thus the definition: In designing an optimal die for a given material, temperature mandrel speed and friction the safe operating condition is such that the specific draw stress (line stress ratio) must be less than 1.

In the Battelle[1] report, it was shown that, in general, the influence of work or strain hardening, temperature and mandrel speed does not appreciably effect the shape of the optimal die. However, as noted above, failure is heavily dependent on these factors. Shown in Figures 3 and 4 are the drawing limit diagrams for 1045 steel for a wide range of frictional conditions. The ordinate is the specific draw stress, the absissa reduction in area in a single pass. In Figure 3 the mandrel friction was constant and the shell die friction varied. The reverse is true of Figure 4. It may be noted that: Regardless of frictional conditions, 40-42% is the largest possible single pass cold draw reduction on a 105mm shell. Also: Reducing the friction between shell and die increases the maximum reduction which can be taken. However, increasing the friction between shell and mandrel increases the maximum reduction which can be taken.

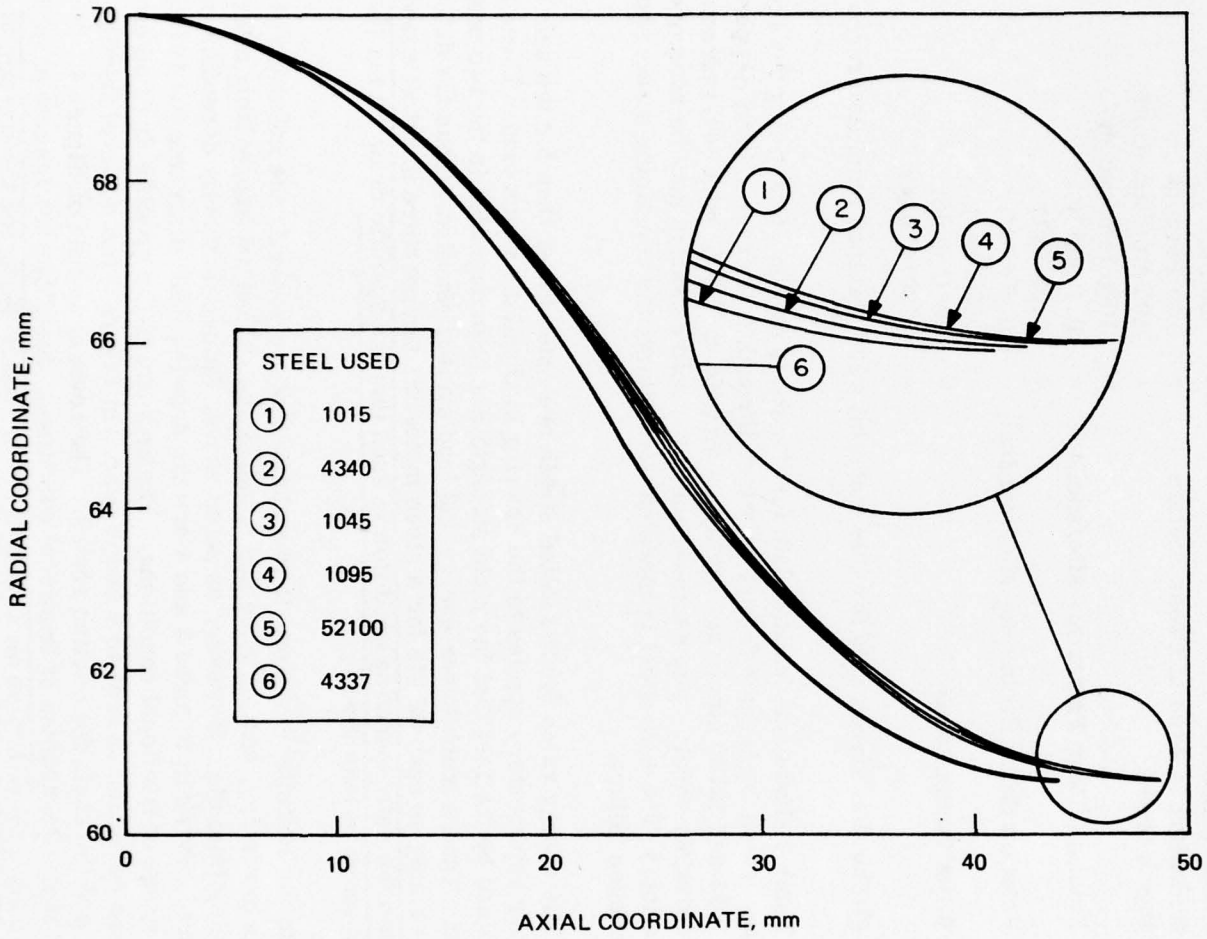

Figure 2. Optimal Die Contours for Various Steels in a Single Pass 40% Draw (See Table 1)

Table 2. R And Z Coordinates For Optimal Die Contours Shown in Figure 2.

STEEL	1015		1045		1095		4337		4340		52100	
	Z	R	Z	R	Z	R	Z	R	Z	R	Z	R
	0	70.000	0	70.000	0	70.000	0	70.000	0	70.000	0	70.000
	6.818	69.630	6.968	69.625	6.941	69.631	6.502	69.618	6.861	69.629	6.940	69.631
	12.500	68.748	12.775	68.732	12.724	68.752	11.921	68.706	12.579	68.745	12.724	68.752
	17.046	67.652	17.420	67.622	17.351	67.660	16.255	67.569	17.154	67.647	17.351	67.660
	20.455	66.590	20.905	66.546	20.822	66.603	19.506	66.464	20.584	66.582	20.821	66.603
	22.728	65.761	23.227	65.708	23.135	65.779	21.674	65.599	22.871	65.752	23.135	65.779
	23.864	65.310	24.389	65.251	24.292	65.330	22.757	65.127	24.015	65.299	24.291	65.330
	24.990	64.862	25.511	64.809	25.449	64.881	23.751	64.693	25.144	64.852	25.448	64.881
	27.243	64.040	27.756	63.998	27.762	64.057	25.737	63.901	27.401	64.033	27.761	64.057
	30.623	62.987	31.124	62.959	31.232	62.999	28.717	62.888	30.786	62.982	31.232	62.999
	35.128	61.901	35.614	61.886	35.859	61.908	32.690	61.846	35.300	61.898	35.858	61.908
	40.761	61.027	41.227	61.022	41.643	61.029	37.656	61.010	40.943	61.026	41.642	61.029
	47.520	60.660	47.963	60.660	48.583	60.660	43.615	60.660	47.714	60.660	48.582	60.660

Table 3. Loads, Stresses and Strains in Processing for the Die Contours Shown in Figure 2.

Material	Die Length, mm	Drawing Load, MN	Punch Head Load, MN	Specific Draw Stress	Strain Differential At Exit, m/m	Total Energy Rate, 10^8 N-mm/s
1015	47.52	.703	.583	.953	.1658	.422
1045	47.96	.666	.553	.923	.1625	.399
4337	43.61	.955	.803	1.09*	.1990	.573
4340	47.71	.553	.458	.945	.1643	.332

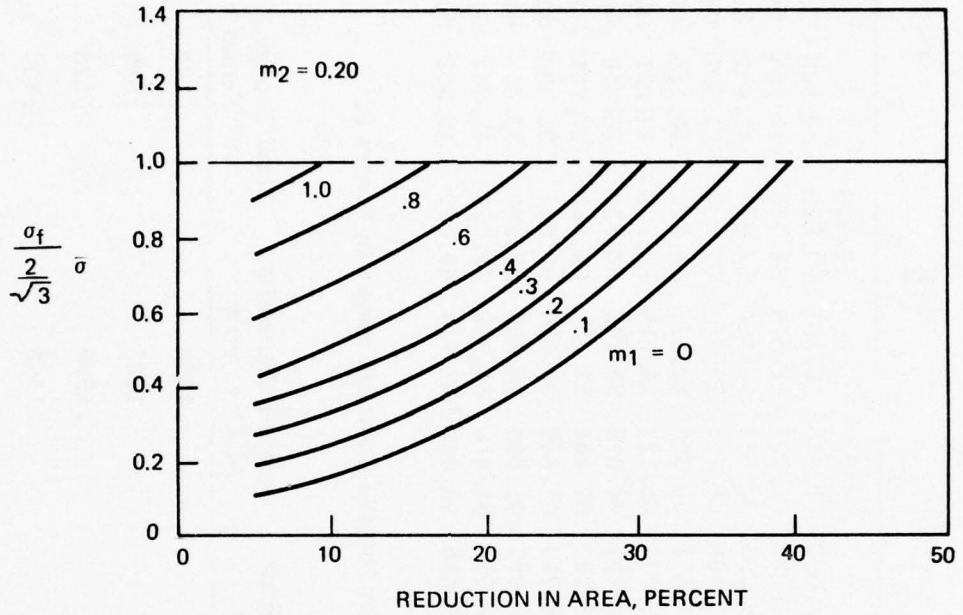

Figure 3. Drawing Limit Diagram for a Constant Friction at the Punch-Material Interface (R_o = 70 mm, r_o = 43 mm, Temperature = 20° C, Curved-Straight-Curved Die Angle = 17.8 Degrees)

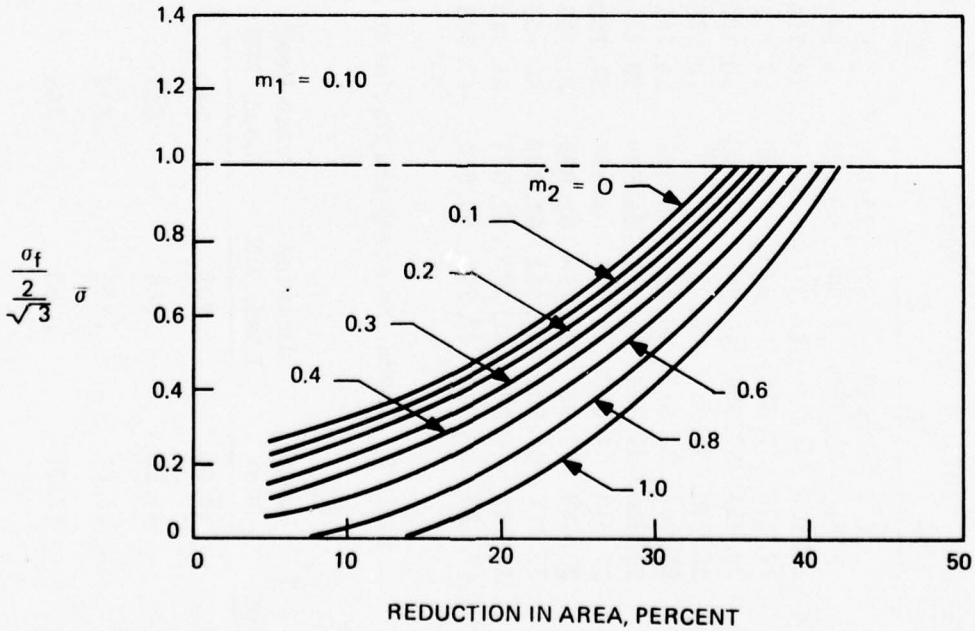

Figure 4. Drawing Limit Diagram for a Constant Friction at the Die-Material Interface (R_o = 70 mm, r_o = 43 mm, Temperature = 20° C, Curved-Straight-Curved Die Angle = 17.8 Degrees)

The effect of friction on shape is shown in Figure 5. Shown are the optimal 40% reduction contours for 1045 steel under extremes of frictional conditions. Curve 1 has the base line friction conditions of Figure 2. Curve 2 represents the desirable quality of decreasing the shell die friction. Curve 3 represents the desirable quality of increasing the friction. The conclusion was that: As in the case of strain-hardening and temperature, friction does not significantly effect the optimal die contour.

Figures 6-14 show the effect of reduction in area on die contours for the drawing of a 1045 steel 105mm billet. Each plot represents the optimal die contour. The computed coordinates are in Table 4, and the failure design data is in Table 5. The specific draw stress data of Table 5 shows, as mentioned above, that 40-42% is the maximum possible reduction in a cold draw. It is also noted that as the areal reduction is increased, the die length, drawing load and punch loads also increase. The drawing load is the total load which must be carried in the shell wall, and the punch load is distributed over the punch face. The effect of increased punch load will, of course, be to reduce tool life. The strain differential column of Table 5 represents the differential in plastic strain between the outermost and innermost fibers in the shell wall at the exit. It is therefore a measure of the strain uniformity in the product wall. As can be noted, an increased areal reduction leads to greater lack of product homogeneity. However, as shown in the Richmond/Devenpeck study, for any reduction the streamlining effect of curved dies will lead to a more uniform product.

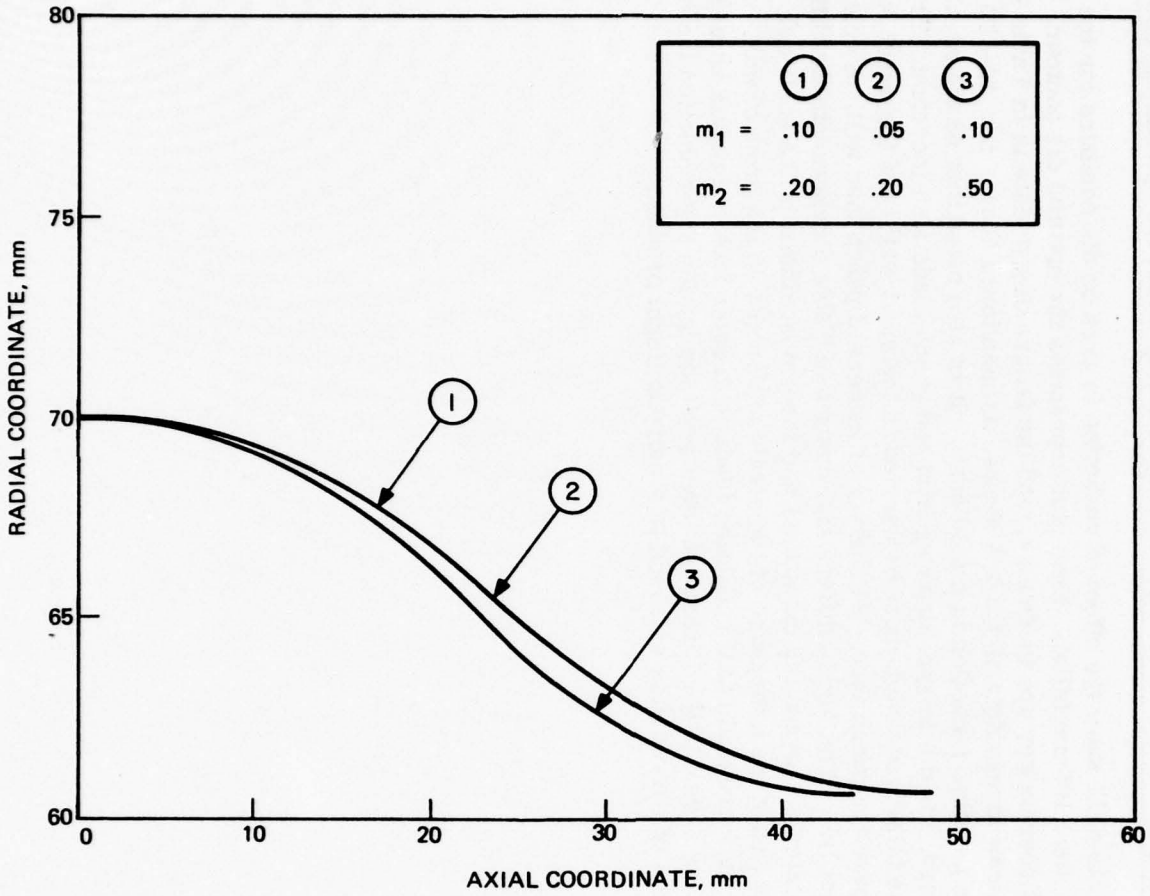

Figure 5. The Effect of Friction on Optimal Die Contour in a Single Pass 40% Draw (See Table 1)

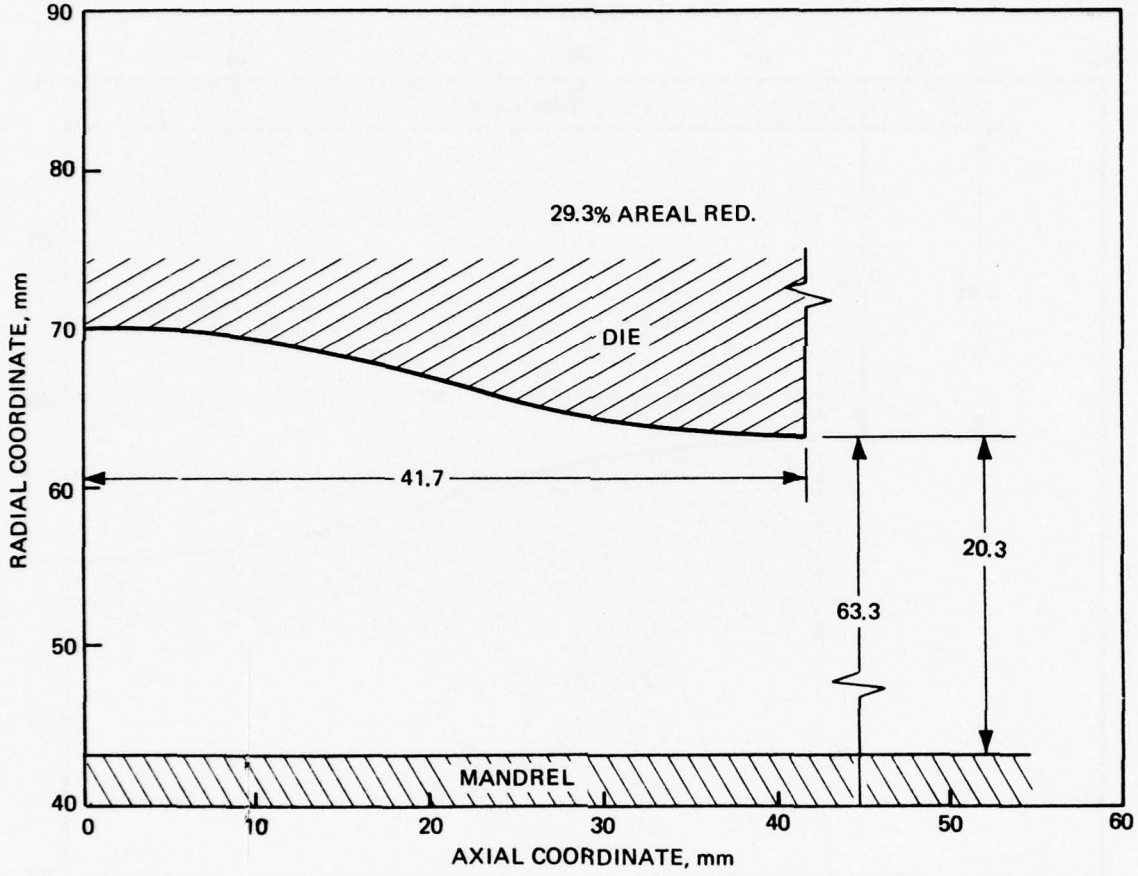

Figure 6. Optimal Die Contours for 1045 Steel in a Single Pass Draw (See Table 1) with Various Reductions

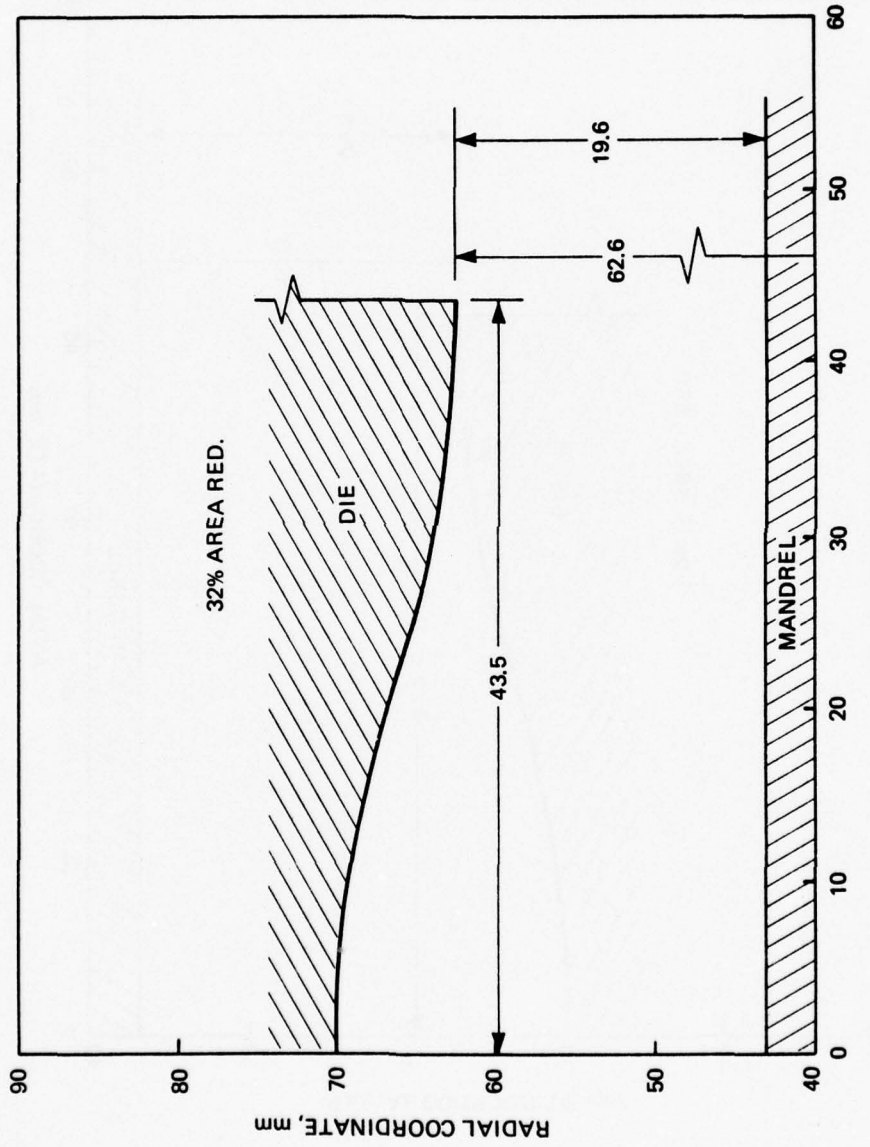

Figure 7. Optimal Die Contours for 1045 Steel in a Single Pass Draw (See Table 1) with Various Reductions.

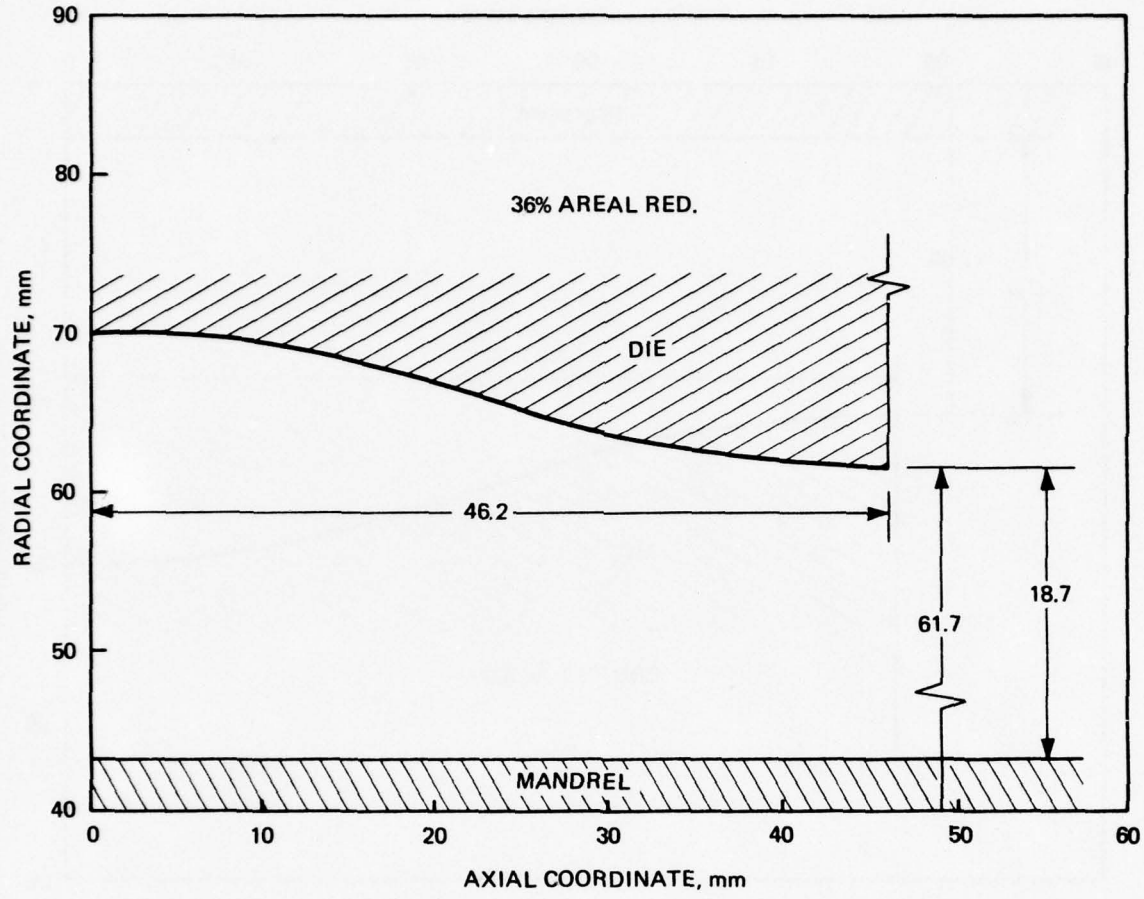

Figure 8. Optimal Die Controus for 1045 Steel in a Single Pass Draw (See Table 1) with Various Reductions.

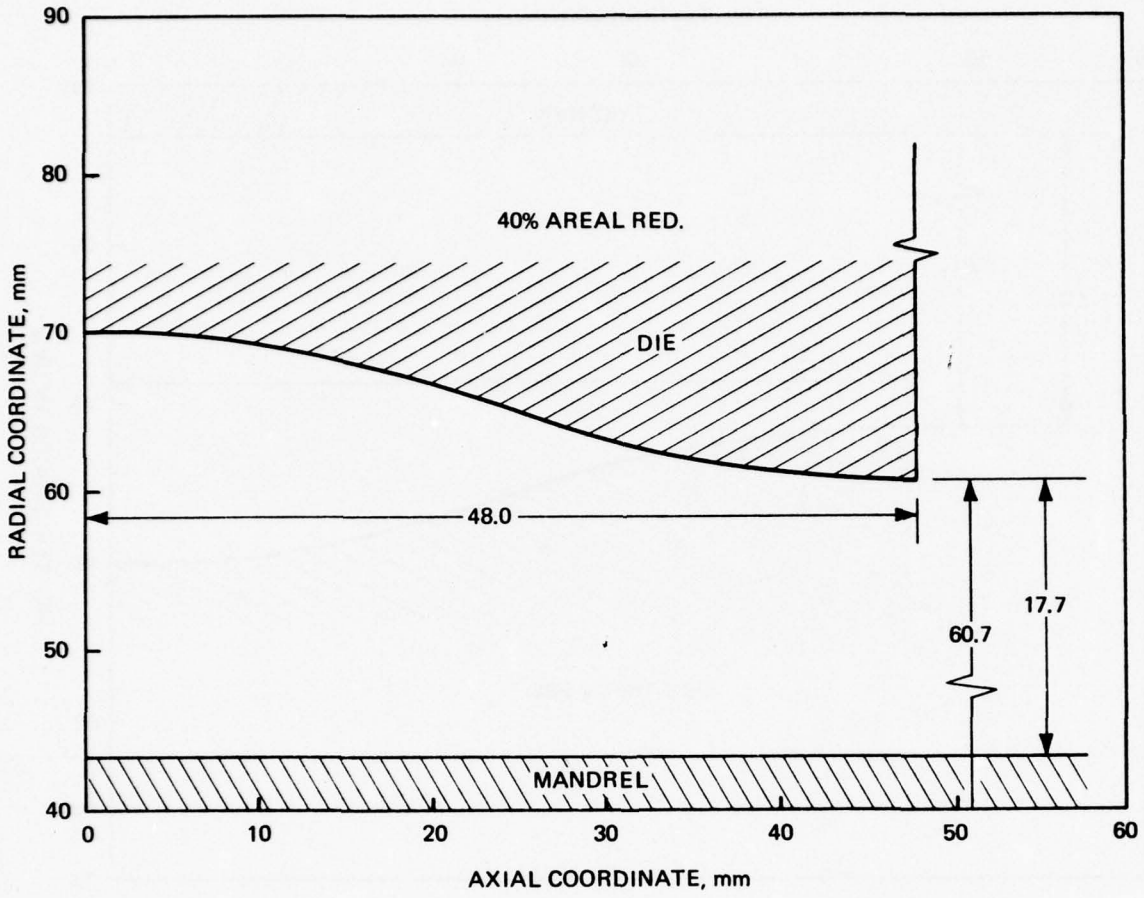

Figure 9. Optimal Die Controus for 1045 Steel in a Single Pass Draw (See Table 1) with Various Reductions.

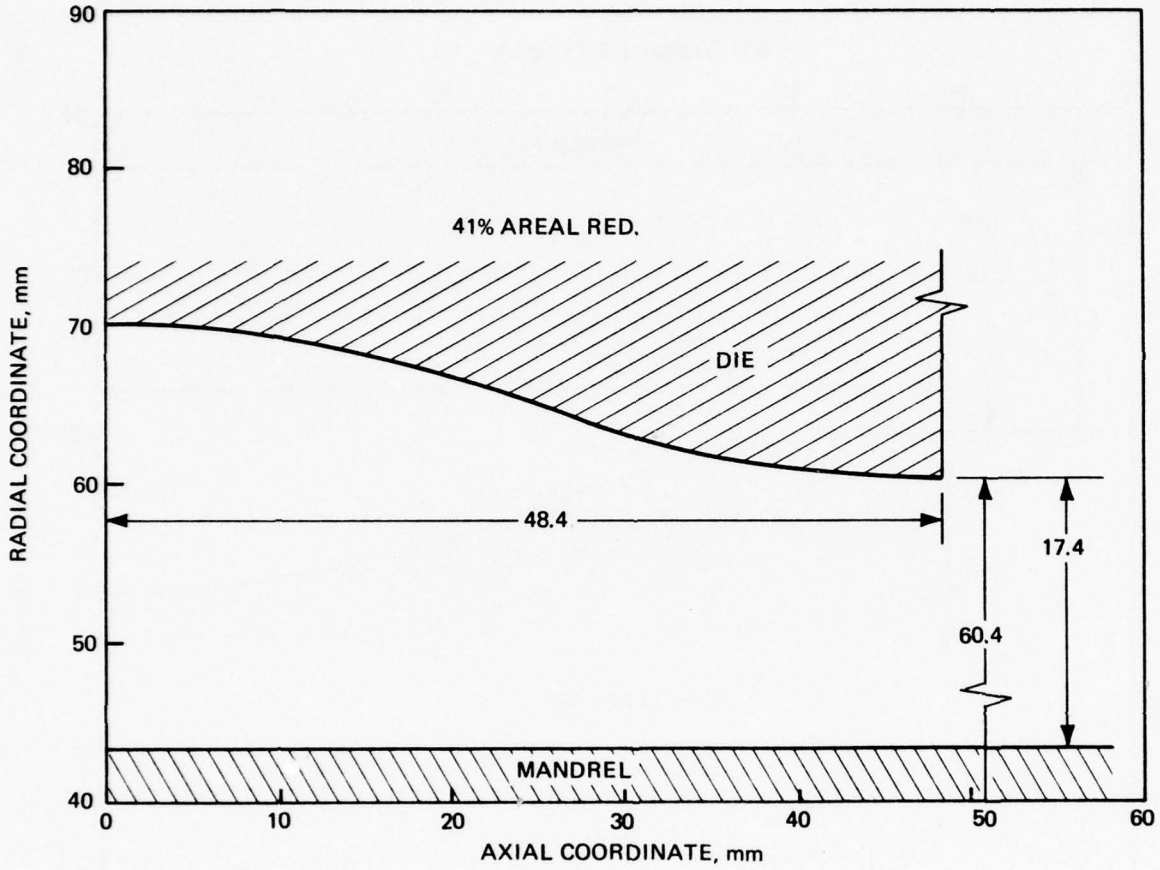

Figure 10. Optimal Die Contours for 1045 Steel in a Single Pass Draw (See Table 1) with Various Reductions.

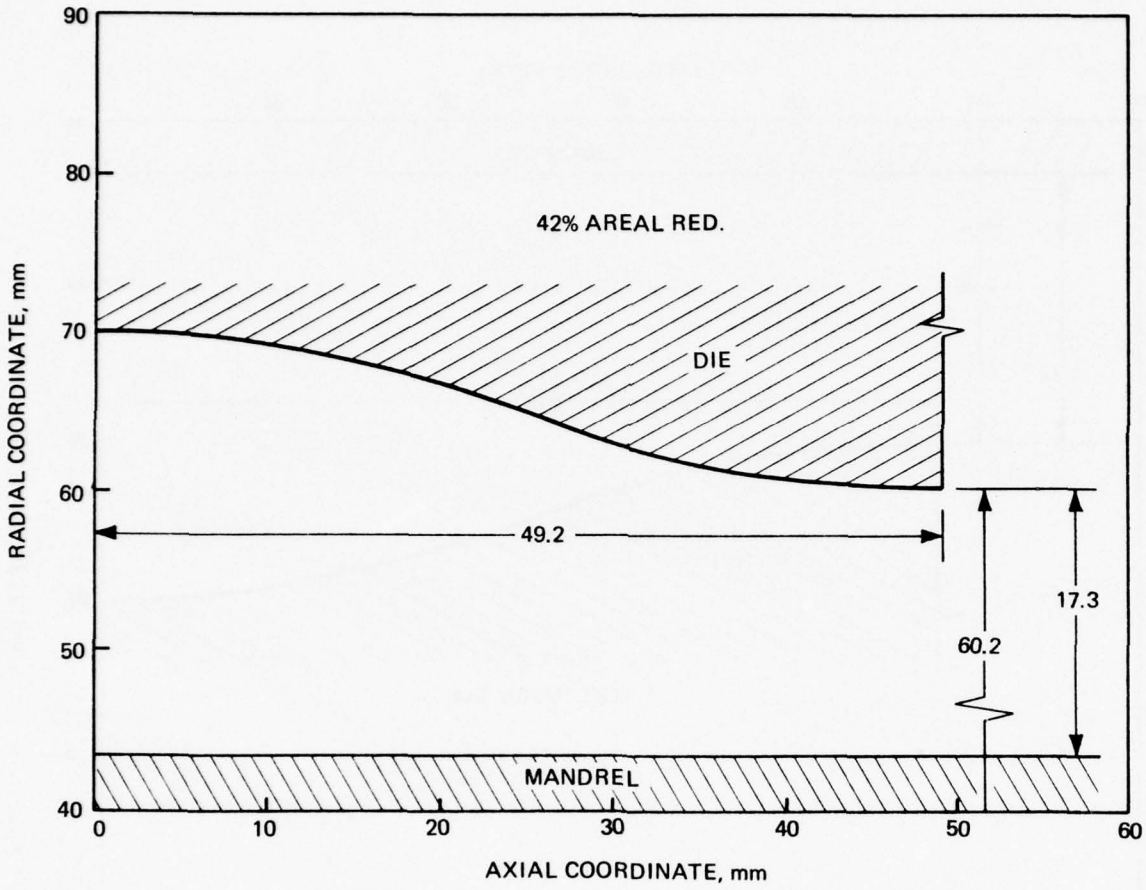

Figure 11. Optimal Die Contours for 1045 Steel in a Single Pass Draw (See Table 1) with Various Reductions.

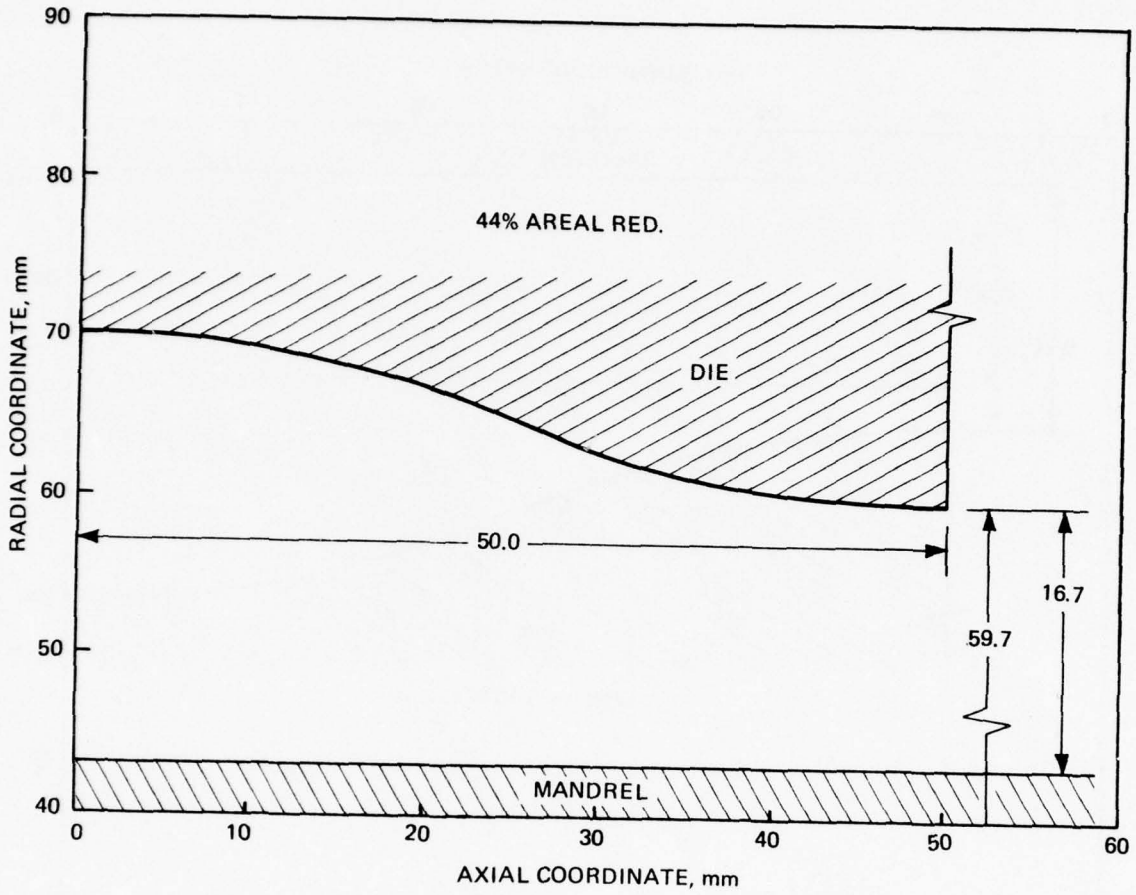

Figure 12. Optimal Die Contours for 1045 Steel in a Single Pass (See Table 1) with Various Reductions.

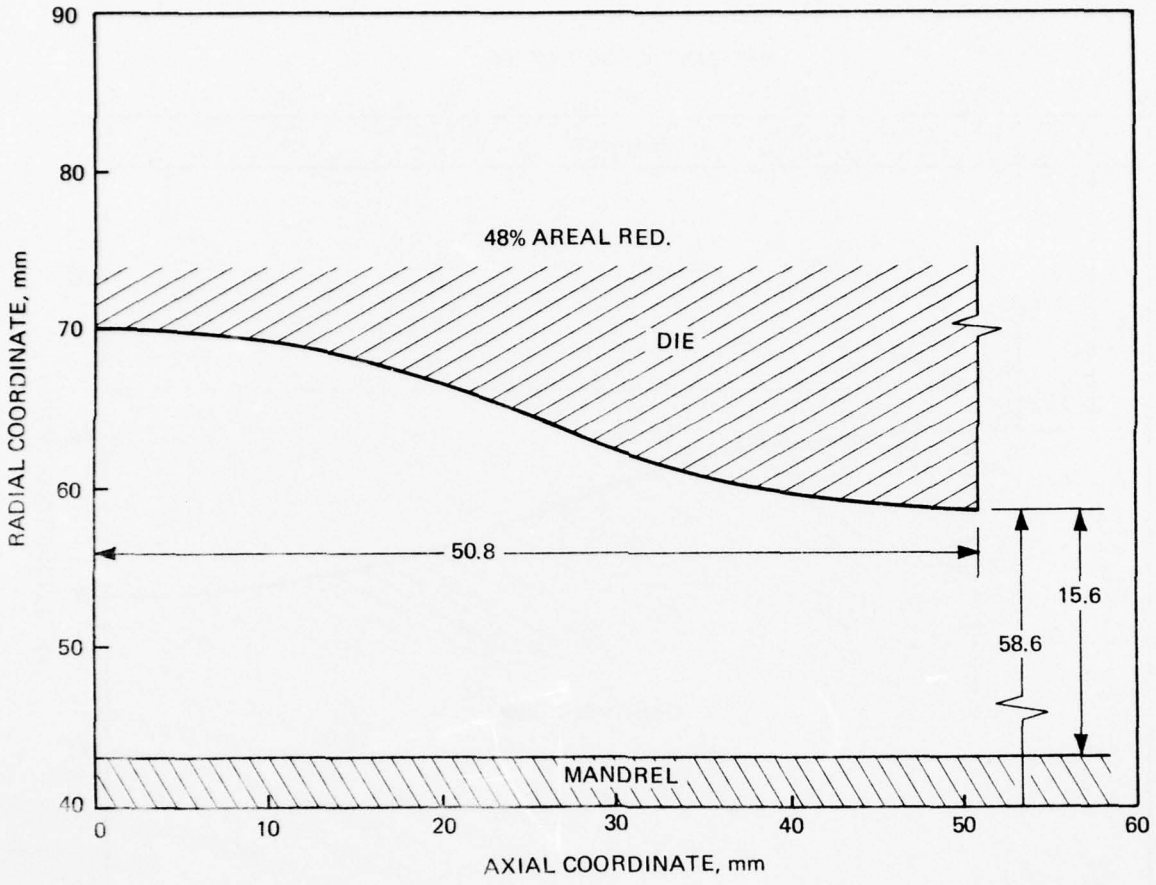

Figure 13. Optimal Die Contours for 1045 Steel in a Single Pass Draw (See Table 1) with Various Reductions.

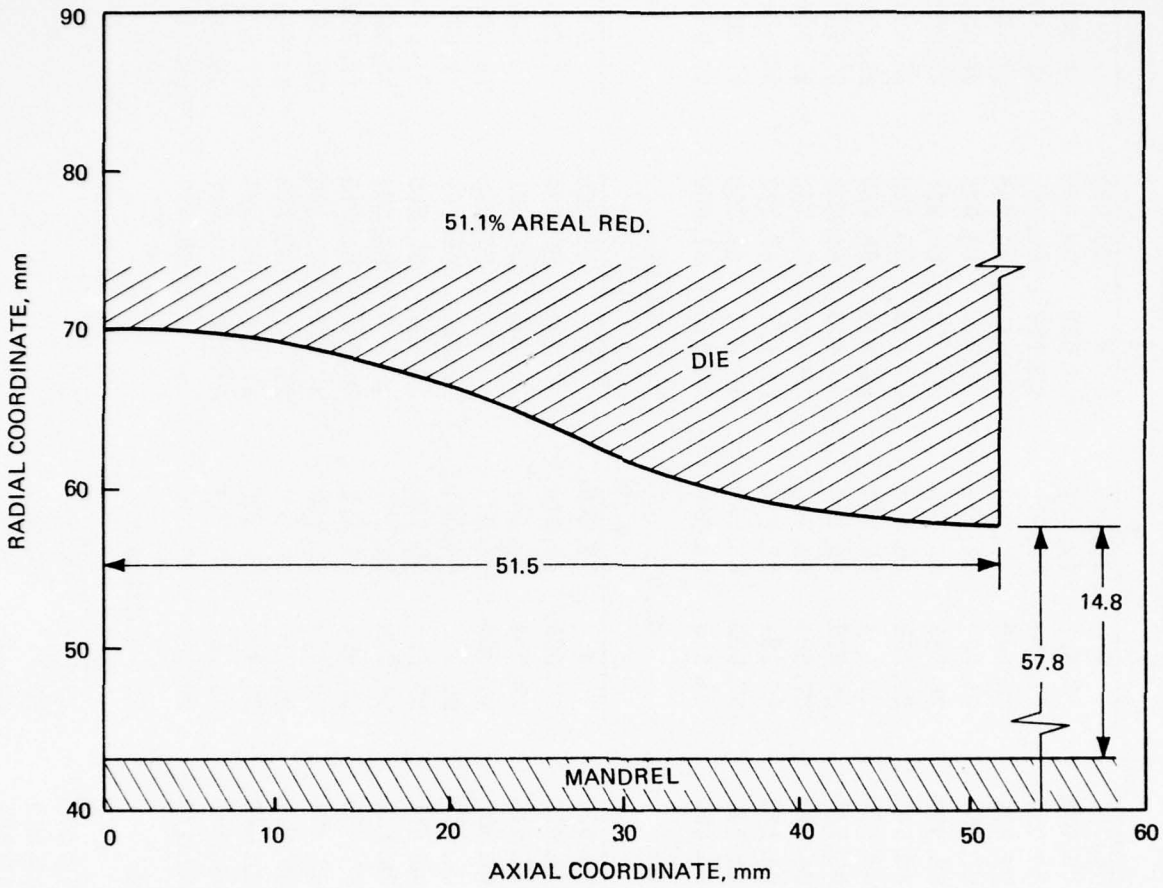

Figure 14. Optimal Die Contours for 1045 Steel in a Single Pass Draw (See Table 1) with Various Reductions.

Table 4. R and Z Coordinates for Optimal Die Contours Shown in Figures 6-14

OPTIMAL DIE CONTOURS

29.3%

Z	r
0	70.00
5.946	69.732
10.901	69.096
14.866	68.309
17.839	67.551
19.821	66.963
20.812	66.643
21.802	66.324
23.782	65.736
26.752	64.979
30.712	64.183
35.661	63.557
41.601	63.290

32.0%

Z	r
0	70.000
6.22	69.707
11.403	69.01
15.549	68.148
18.659	67.316
20.732	66.669
21.769	66.318
22.804	65.967
24.876	65.301
27.982	64.490
32.124	63.628
37.302	62.933
43.515	62.640

36.0%

Z	r
0	70.000
6.608	69.669
12.115	68.882
16.521	67.905
19.825	66.962
22.027	66.227
23.129	65.828
24.229	65.429
26.429	64.695
29.730	63.753
34.131	62.777
39.632	61.990
46.233	61.660

40.0%

Z	r
0	70.000
6.968	69.625
12.775	68.732
17.420	67.622
20.905	66.546
23.227	65.708
24.389	65.251
25.511	64.809
27.756	63.998
31.124	62.959
35.614	61.886
41.227	61.022
47.963	60.660

41.0%

Z	r
0	70.000
7.034	69.616
12.896	68.699
17.586	67.558
21.103	66.453
23.448	65.591
24.620	65.120
25.752	64.606
28.015	63.834
31.410	62.767
35.937	61.666
11.596	60.781
18.387	60.410

42.0%

Z	r
0	70.000
7.066	69.610
12.954	68.680
17.664	67.523
21.197	66.401
23.552	65.525
24.729	65.047
25.894	64.575
28.223	63.709
31.716	62.600
36.374	61.455
42.197	60.536
49.184	60.150

44.0%

Z	r
0	70.000
7.309	69.584
13.400	68.591
18.273	67.355
21.928	66.154
24.364	65.216
25.583	64.704
26.745	64.215
29.071	63.320
32.559	62.175
37.210	60.994
43.023	60.047
49.999	59.650

48.0%

Z	r
0	70.000
7.359	69.549
13.492	68.471
18.398	67.124
22.077	65.813
24.530	64.784
25.757	64.221
26.948	63.675
29.33	62.676
32.903	61.402
37.667	60.095
43.612	58.048
50.768	58.610

51.1%

Z	r
0	70.000
7.480	69.519
13.713	68.367
18.700	66.926
22.440	65.517
24.933	64.411
26.179	63,804
27.387	63.216

51.1 (Continued)

Z	r
29.804	62.144
33.428	60.779
38.260	59.382
44.300	58.266
51.548	57.800

Table 5. Loads, Stresses and Strains in Processing for the Dies of Figures 6-14.

AISI 1045 Steel, 20° C Draw Temperature

Areal Red., %	Die Length, mm	Drawing Load, MN	Punch Head Load, MN	Specific Draw Stress	Strain Differential at Exit, m/m	Total Energy Rate 10^8 N-mm/s
29.3	41.60	.456	.362	.542	.1533	.3223
32.0	43.51	.504	.405	.621	.1544	.3431
36.0	46.23	.582	.474	.757	.1555	.3724
40.0	47.96	.666	.553	.923	.1625	.3998
41.0	48.39	.688	.573	.970	.1629	.4062
42.0	49.18	.712	.594	1.018*	.1641	.4128
44.0	50.00	.758	.638	1.121*	.1662	.4248
48.0	50.77	.861	.737	1.373*	.1790	.4475
51.1	51.55	.947	.830	1.603*	.1875	.4630

II CONVENTIONAL TAPERED DIES

In order to address the problems of simulation and failure in conventional dies, a computer program SHELL has been developed. A mathematical summary is given in Appendix A. The purpose of this section is to present guidelines for designing tapered dies which will not permit material failure (punch-through).

Table 6 indicates the baseline process variables being used. Changes in these quantities are noted when appropriate. Figures 15 and 16 are drawing limit diagrams for a cold, 40% reduction of AISI 1045 billet with various die angles. These figures plot specific draw stress vs die semi angle. As in curved dies, when the specific draw stress is unity failure occurs. Figure 15 shows that, for any level of friction between shell and die, increasing the die angle avoids failure. Decreasing the shell-die friction enhances the process. Figure 15 also demonstrates that for any friction level there is a minimum angle to avoid failure. Figure 16 shows the effect of varying μ_2, the shell mandrel friction. Increasing this friction enhances the process in that failure cannot occur. Noting that drawing with zero or negative draw stress that there is a minimum angle below which drawing cannot occur.

Table 6. Conditions Used for Theoretical Determination of Process Variables in Conventional Dies

Billet Material	=	AISI 1045 Steel (*)
Billet Outside Diameter	=	140 mm (**)
Billet Inside Diameter	=	86 mm (**)
Punch Diameter	=	86 mm (**)
Reduction in Area of Cross Section	=	40 Percent (**)
Punch Speed	=	100 mm/sec [cold]
	=	1000 mm/sec [hot]
Friction Coefficient, μ_1 (shell/mandrel)	=	0.1 [cold]
	=	0.25 [hot]
Friction Coefficient, μ_2 (shell/die)	=	0.2 [cold]
	=	0.35 [hot]
Billet Temperature	=	20° C [cold]
	=	1000° C [hot]
Die Half Angle α	=	Variable

(*) The flow stress data for this material were obtained from Reference 29.

(**)These vary with reduction in area.

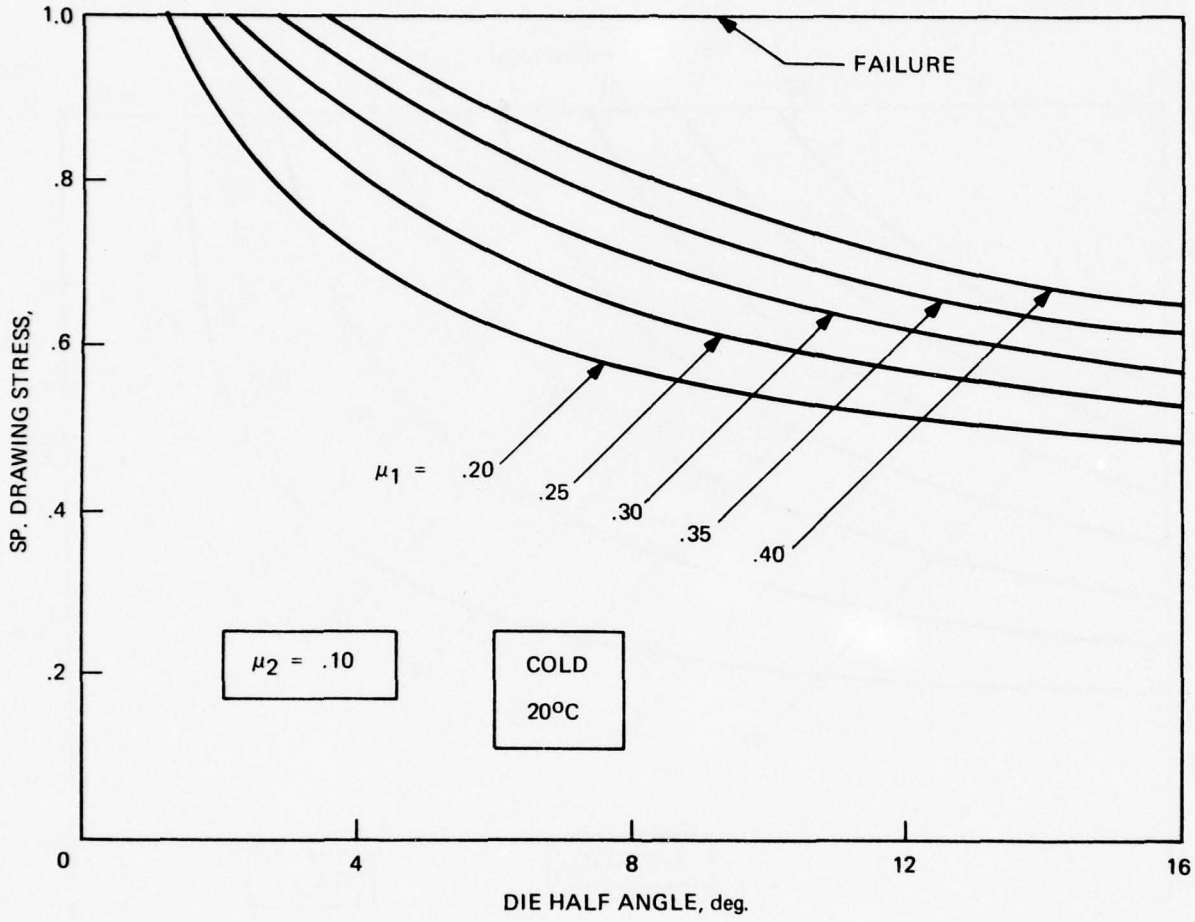

Figure 15. Specific Draw Stress vs. Die Half Angle for Various Processing Conditions.

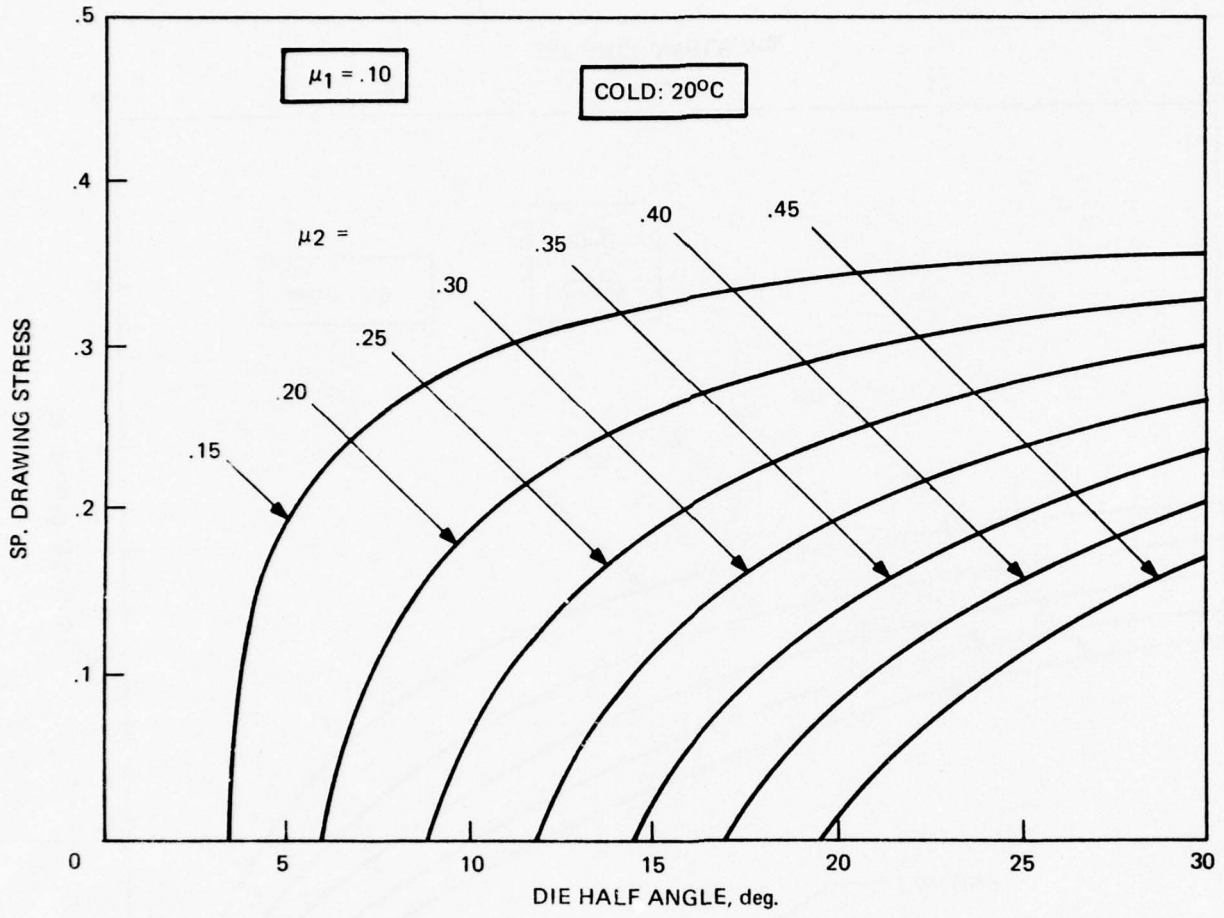

Figure 16. Specific Draw Stress vs. Die Half Angle for Various Processing Conditions.

Figure 17 and 18 present an analagous study to the one above, except that drawing was performed at 1000° C. Comparison of Figures 15 and 17 shows that hot drawing is a similar process except that the sp. draw stress is lower. A comparison of Figures 16 and 18 shows that in both hot and cold drawing, increased mandrel friction is beneficial to avoiding failure.

The effect of the punch velocity on cold drawing is shown in Figure 19. The plot of specific draw stress vs semiangle at six punch velocities is shown. All curves coincide. This may be explained in terms of the materials properties in Table 7. Table 7 shows the dependence of the metals used in this on strain hardening and strain rate sensitivity. Strain hardening is covered by assuming that the equivalent plastic stress (σ) is proportional (k) to the plastic strain raised to a power (n). This is seen to be true for cold to warm (400-500° C) temperatures. In this range the value of k and n is somewhat influenced by strain rate. For temperatures above 600° C, the above law is not valid. In this range a better assumption is that the stress ($\bar{\sigma}$) is proporational (c) to the strain rate ($\dot{\bar{\epsilon}}$). The values of c and n depend upon the level of strain. Since the velocity of the punch defines the level of strain rate it should be anticipated that, at higher temperatures, this factor is important, and, conversely at lower temperatures unimportant.

Figure 19 indicates the general conclusion that the punch velocity does not influence cold drawing.

Figure 20 shows the influence of punch velocity in a 40% hot (1000° C) draw with moderate friction and punch velocities from 100 to 1000 mm/s. The trend is the same as in cold drawing.

An additional effect of temperature for a low speed draw is illustrated in Figure 21. Shown is the drawing limit diagram for a 100 mm/s draw over a range of temperatures from 50° C to 1000° C. It is seen that up to about 500° C, the cold-warm range, the temperature has no effect, and the specific draw stress is constant with increasing half angle. Between 500° C and 1000° C the specific draw stress is lowered by about 10%, and the drawing curve is parallel to the cold curve. Beyond 1000° (not shown) the behavior is nonlinear. As the molten state is approached the draw stress drops and, as should be expected, drawing is not possible.

A corresponding study for a high punch speed is shown in Figure 22. The punch speed is 1000 mm/s, ten times that of Figure 21. Up to about 1000° C the material response is essentially the same as in drawing at 100 mm/sec.

A final comparison between hot and cold drawing is displayed in Figures 23 and 24. As is shown in Figure 23 when the coefficients of friction are equal, irrespective of their value, the curve is a horizontal line. This is the one circumstance in cold drawing under which the die angle is not important. Figure 24 shows a similar study at 1000° C as can be seen as the same as for a cold draw.

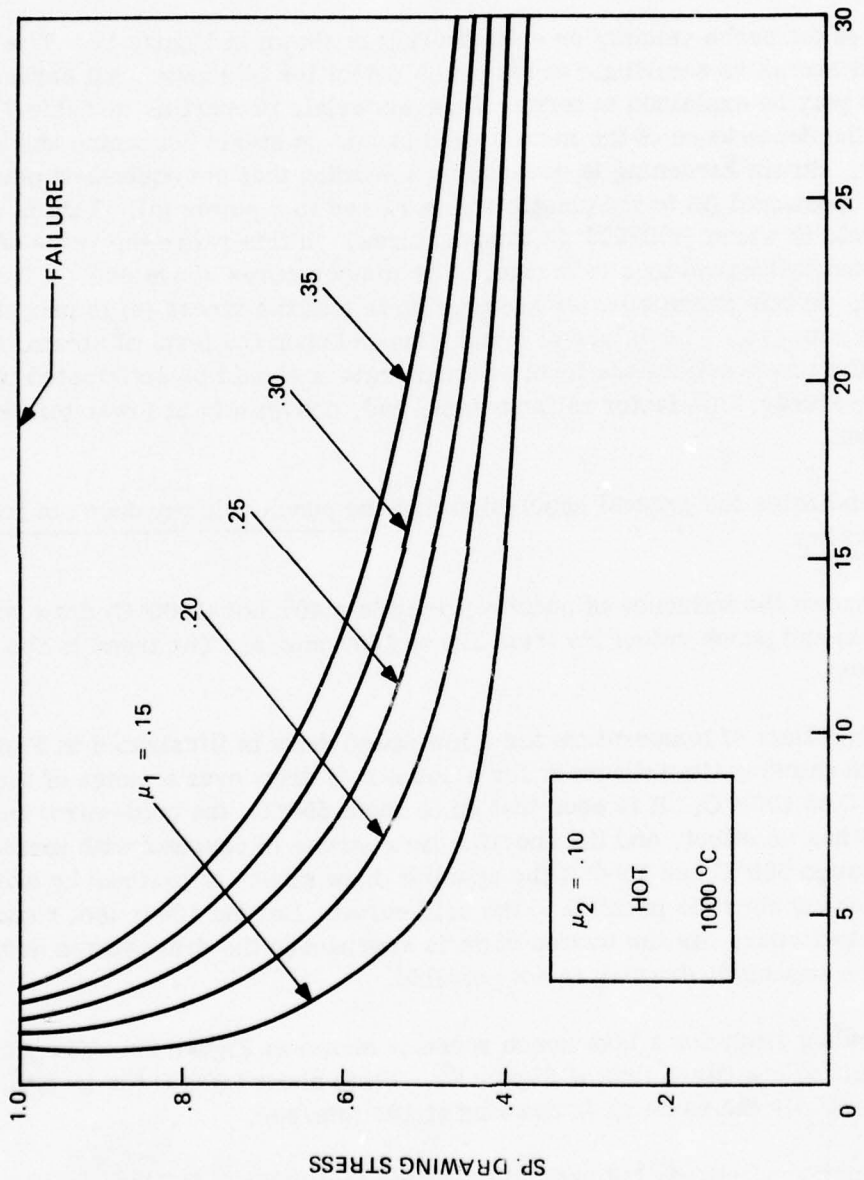

Figure 17. Specific Draw Stress vs. Die Half Angle for Various Processing Conditions.

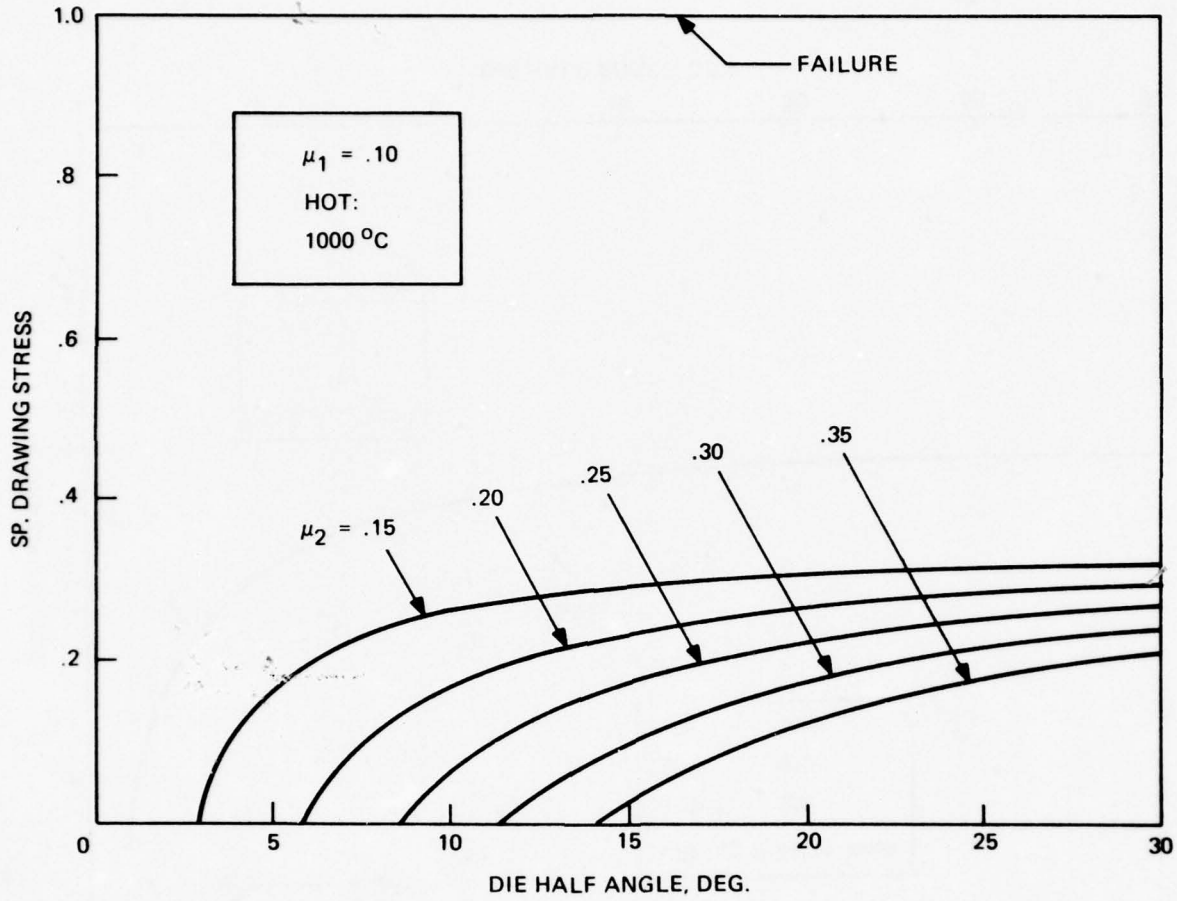

Figure 18. Specific Draw Stress vs. Die Half Angle for Various Processing Conditions.

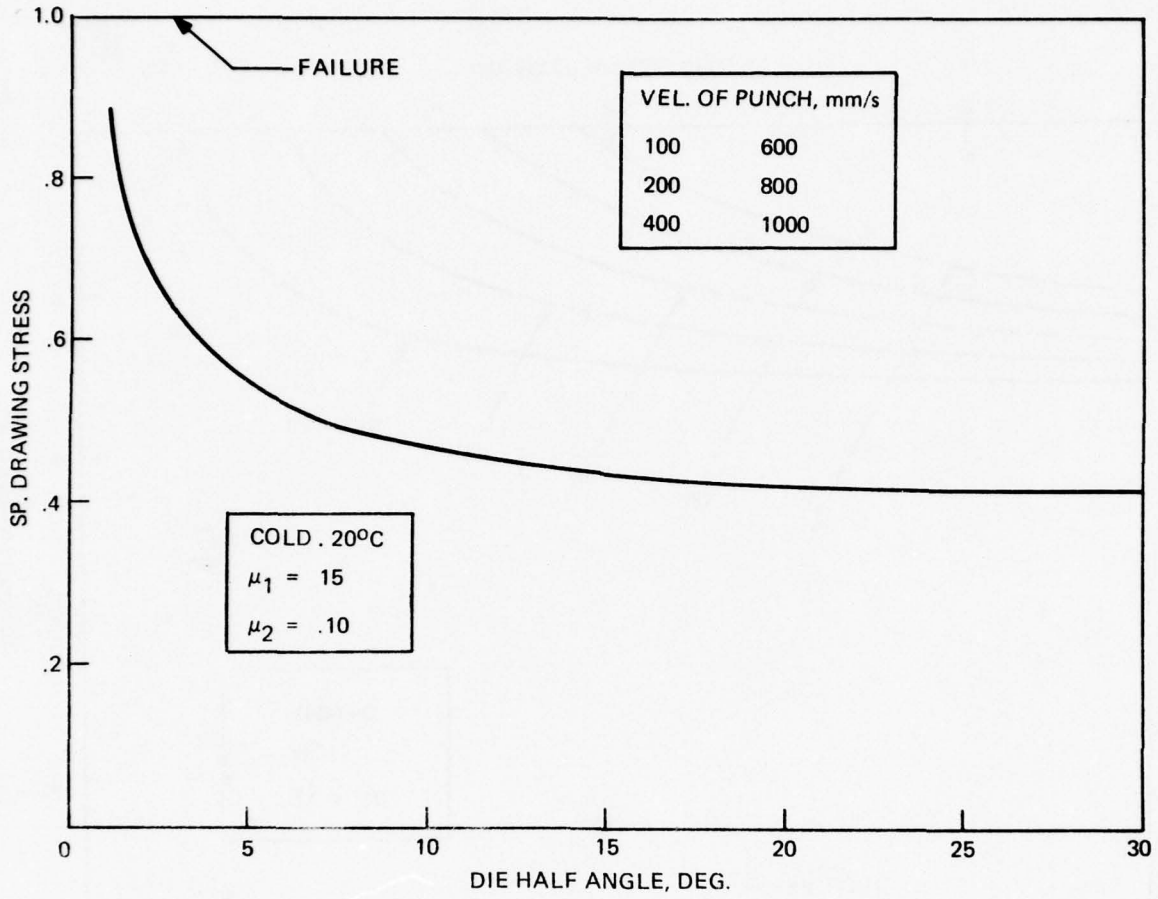

Figure 19. Specific Draw Stress vs. Die Half Angle for Various Processing Conditions.

Table 7. Material Properties

I. Cold (20° C) Drawing

$\bar{\sigma} = K (\bar{\epsilon})n$

Steel	Strain Rate, 1/s	K_D 10^3 psi	n
1015	1.6	113.8	.10
1045	1.6	147.9	.11
1045	1.5	137.9	.14

II. Hot (600° C) Drawing

$\bar{\sigma} = C (\dot{\bar{\epsilon}})^m$

Steel	Strain↓	600°		800°		1000°		1200° ←		Temp° C
		c	m	c	m	c	m	c	m	
1015	.2	36.8	.112							
1015	.25			19.9	.105	17.0	.045	7.2	.137	
1015	.4	40.6	.131							
1015	.5			21.5	.104	18.8	.058	6.8	.169	
1015	.6	40.0	.121							
1015	.7	39.5	.114	21.1	.109	18.3	.068	5.7	.181	
		900°		1000°		1100°		1200° ←		Temp° C
		c	m	c	m	c	m	c	m	
1045	.05	25.4	.080	15.1	.089	11.2	.100	8.0	.175	
1045	.10	28.9	.082	18.8	.103	13.5	.125	9.4	.168	
1045	.20	33.3	.086	22.8	.108	15.4	.128	10.5	.167	
1045	.30	35.4	.083	24.6	.110	15.8	.162	10.8	.180	
1045	.40	35.4	.105	24.7	.134	15.5	.173	10.8	.188	
1095	.10	18.3	.146	13.9	.143	9.8	.159	7.1	.184	
1095	.30	21.9	.133	16.6	.132	11.7	.147	8.0	.183	
1095	.50	21.8	.130	15.7	.151	10.6	.176	7.3	.209	
1095	.70	21.0	.128	13.6	.179	9.7	.191	6.5	.232	
4337	.10	22.1	.080	16.6	.109	12.1	.115	8.2	.165	
4337	.30	28.1	.077	20.8	.098	15.0	.111	10.7	.138	
4337	.50	29.2	.075	21.8	.096	15.7	.112	11.3	.133	
4337	.70	28.1	.080	21.3	.102	15.5	.122	11.3	.135	
52100	.10	20.9	.123	14.3	.146	9.5	.169	6.7	.203	
52100	.30	25.5	.107	17.7	.127	12.0	.143	8.3	.171	
52100	.50	25.9	.107	17.7	.129	12.3	.143	8.3	.178	
52100	.70	23.3	.131	16.8	.134	12.0	.148	7.7	.192	

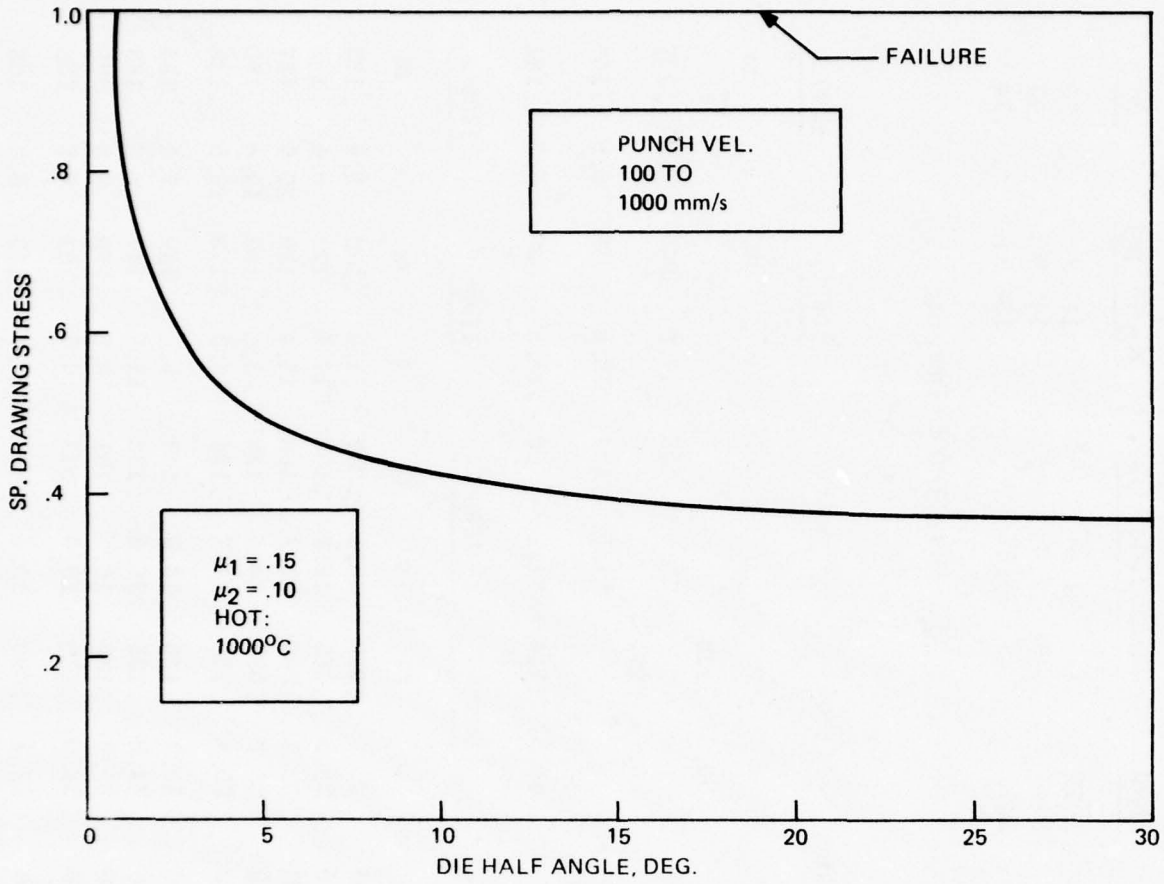

Figure 20. Specific Draw Stress vs. Die Half Angle for Various Processing Conditions.

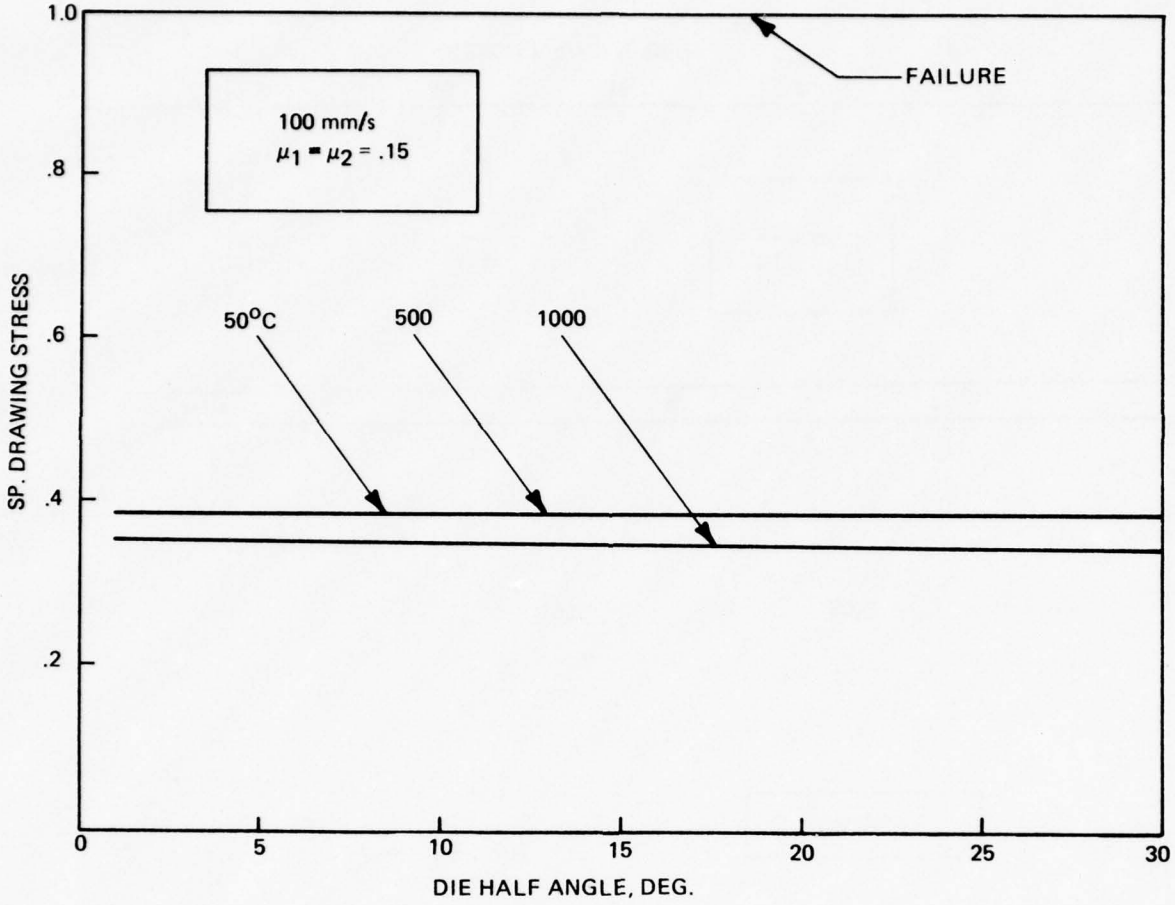

Figure 21. Specific Draw Stress vs. Die Half Angle for Various Processing Conditions.

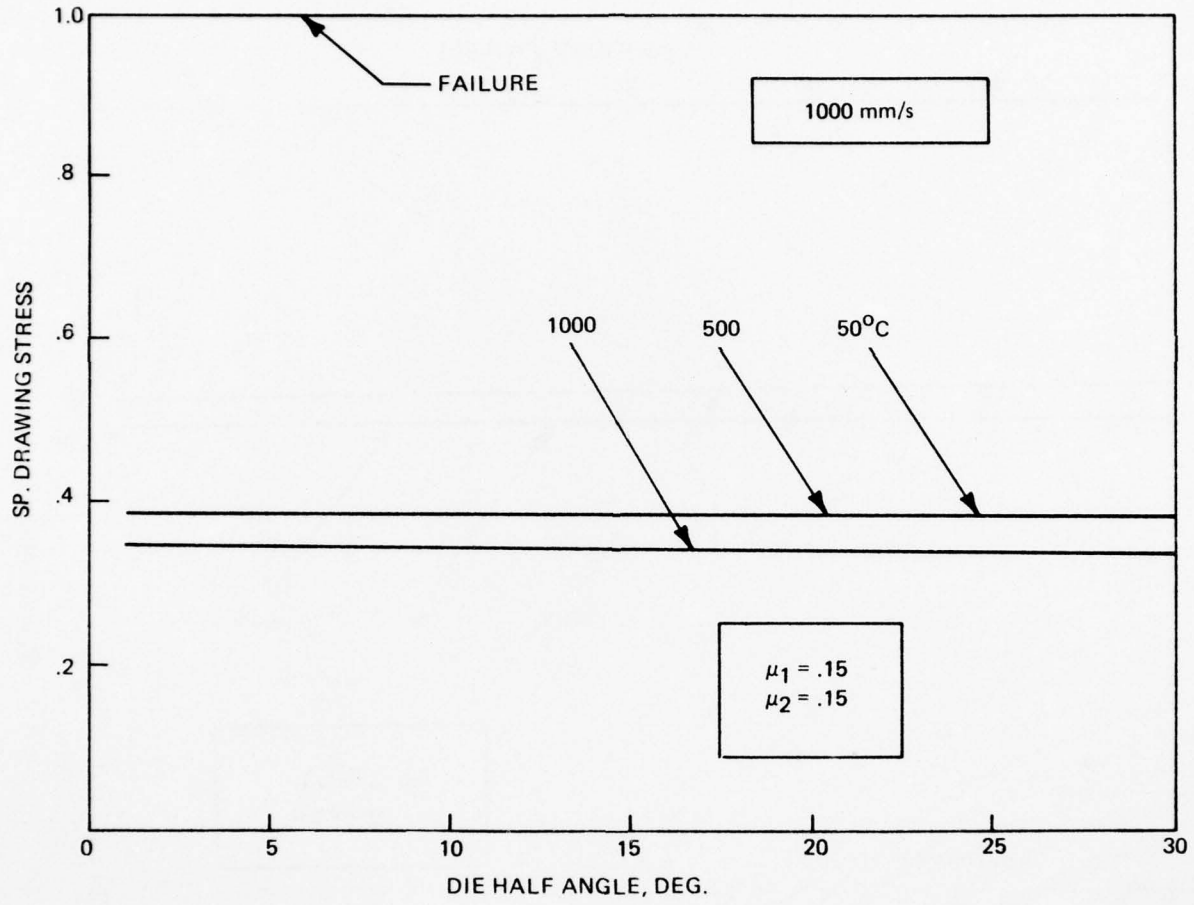

Figure 22. Specific Draw Stress vs. Die Half Angle for Various Processing Conditions.

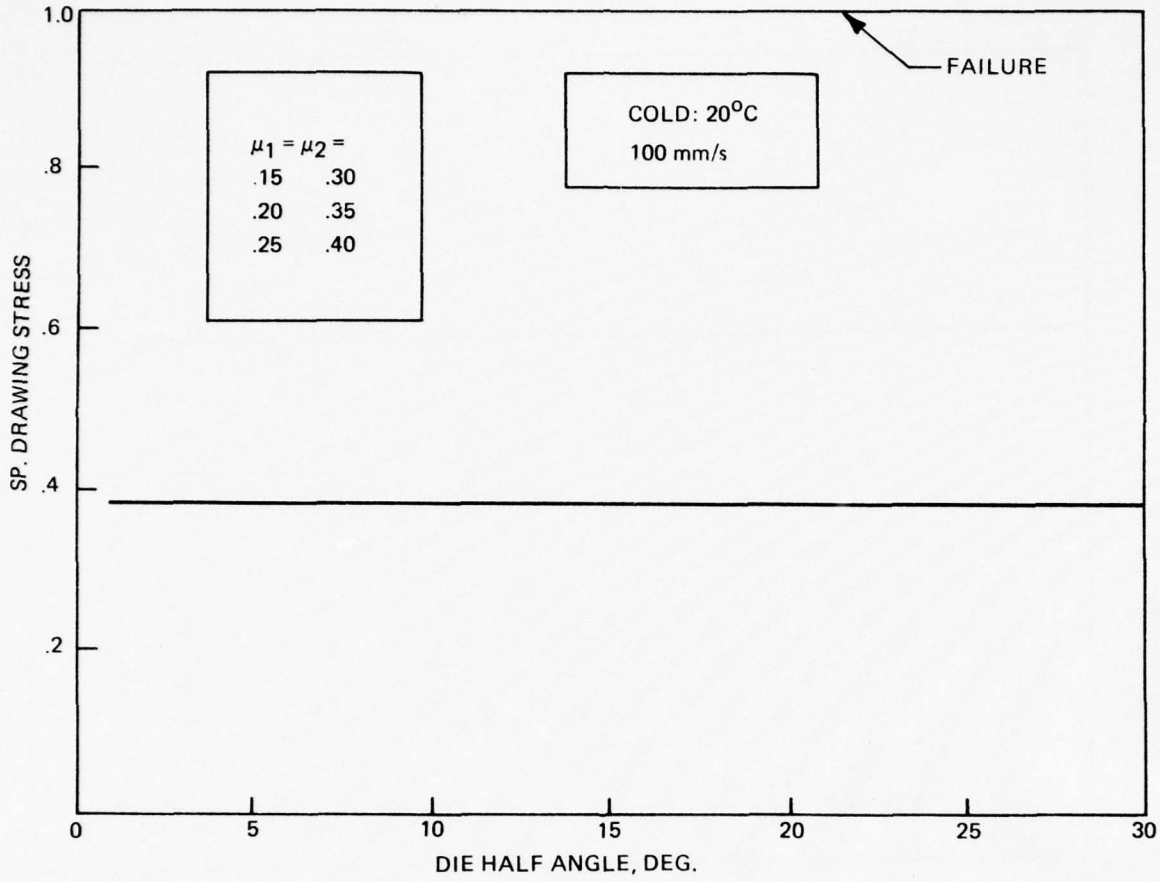

Figure 23. Specific Draw Stress vs. Die Half Angle for Various Processing Conditions.

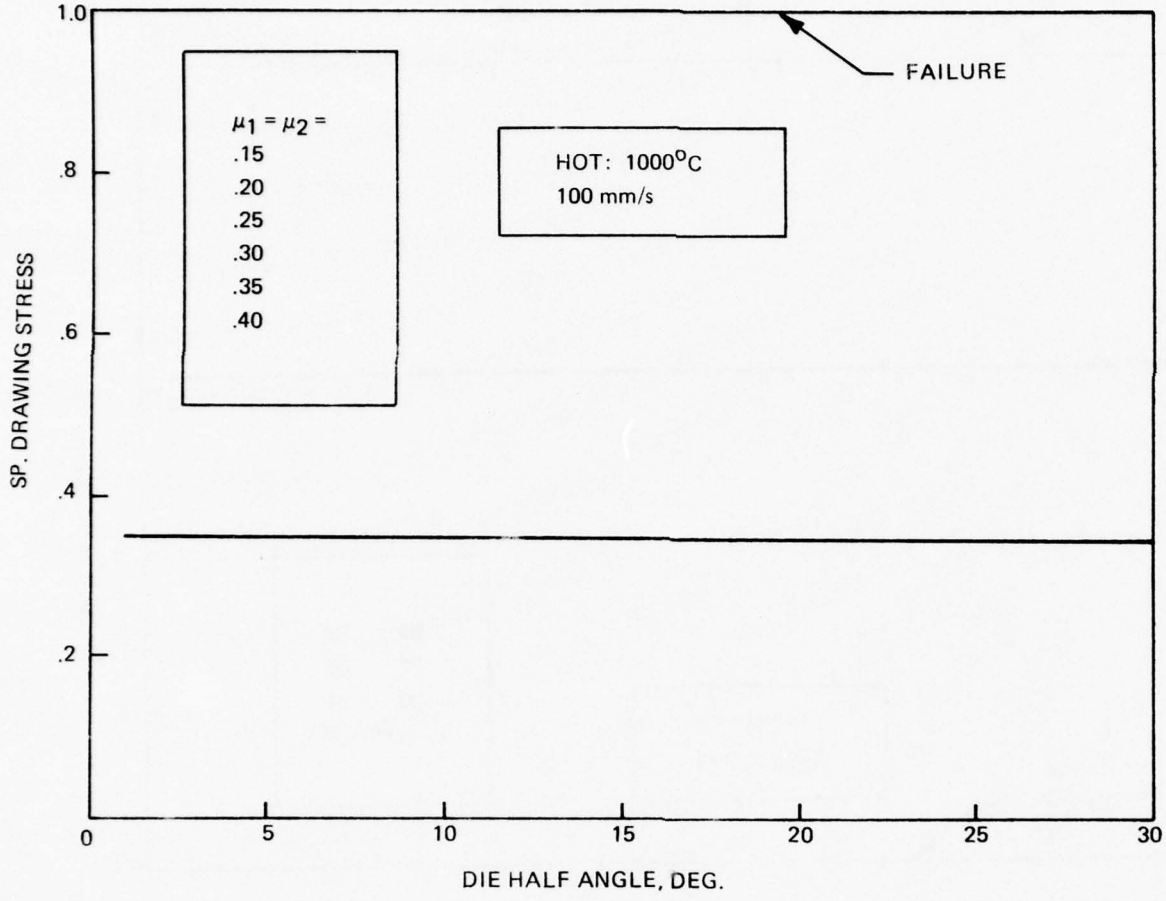

Figure 24. Specific Draw Stress vs. Die Half Angle for Various Processing Conditions.

It should be noted with caution that much of the above study was performed with the two coefficients of friction equal. In practice this equality condition is seldom seen. The striking similarity shown between cold and hot forming will hold only in this restricted condition. As can be noted from Figure 16 and 18, when the two coefficients differ this results in a larger difference between hot and cold drawing. This difference manifests itself as a reduced stress in hot drawing.

III HEAT TRANSFER IN DRAWING

As mentioned in the Battelle study and in the Appendix to this report, a study of the effects of heat conduction during hot drawing was undertaken. In drawing both plastic flow and friction contribute to heat generation. About 90-95% of the mechanical press energy expended in forming will appear as heat. As was seen in Section II above, temperature at higher speeds is the principal factor in failure. The mathematical model used to predict the conduction of heat is described in the Battelle[1] report. The computer programs resulting from that report were used to achieve the results given below. The conditions used were for 40% hot reduction of 1045 steel as shown in Table 1.

Figure 25 shows the isotherms (lines of constant temperature) when steady state conditions are reached. The initial billet temperature was (Table 1) 1000° C with a billet velocity of 500 mm/sec. As can be seen the maximum temperature rise is about 30° C in the worked zone as shown: Figure 26 shows a simulation identical to that of Figure 25, except that the speed has been doubled, to 1000 mm/sec. Again the maximum temperature rise is about 30° C. However, as can be noted by the elongated 1030° C isotherm, the higher temperature zone has extended back into the die and forward into the product.

(For convenience, Figure 27 taken from the Battelle report is presented. The processing conditions are identical to that of Figure 26, a punch velocity of 1000 mm/s. The only difference is that the Battelle run was terminated at .145 sec after drawing was initiated, and only about 50% of the product had been formed. Figure was run until about .3 sec, when all material had been processed. The temperature distributions are nearly identical. It was concluded that running only half the material through the die, and, hence half the computer expense, was sufficient for practical purposes).

Figure 28 shows the temperature increase starting with a cold draw (20° C). The punch head velocity was 200 mm/s. The maximum temperature rise is about 320° C, near the punch-shell interface.

Figure 29 shows the temperature distribution in a cold, 40%, draw operation (20° C ambient) at 200 mm/s using an optimal double curvature die. As can be noted by comparing Figures 25 and 30, the maximum temperature rise is higher (by about 50° C) in the curved die.

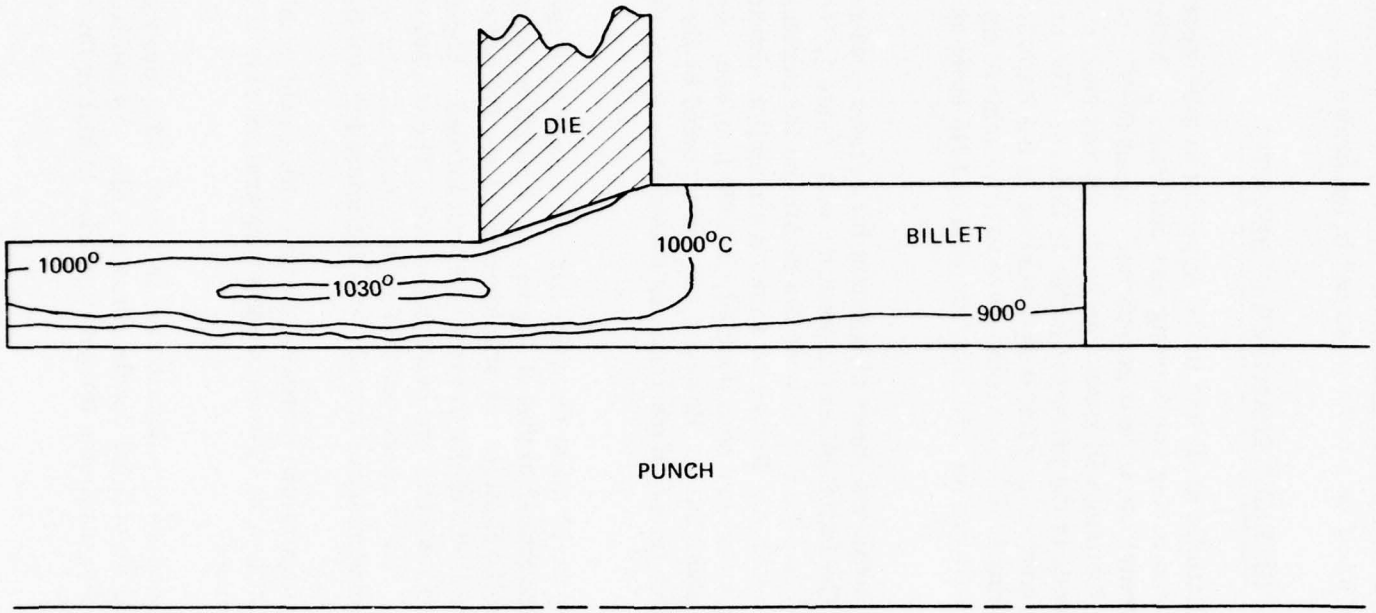

Figure 25. Temperature Distribution in Hot Drawing of Steel Shell Through a Conical Die. (Billet Temperature 1000° C, Tooling Temperature 20° C). Velocity: 500 mm/s.

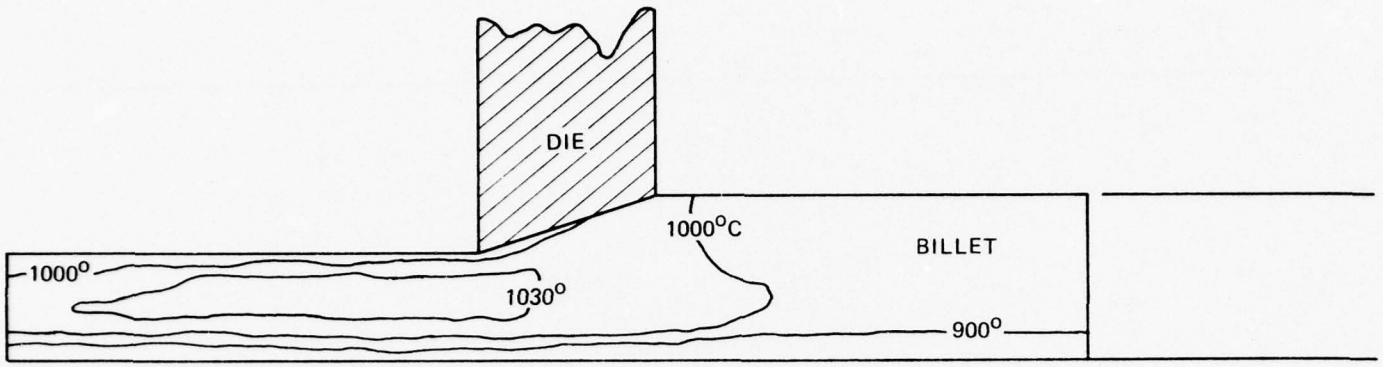

Figure 26. Temperature Distribution in Hot Drawing of Steel Shell Through a Conical Die. (Billet Temperature 1000° C, Tooling Temperature 20° C). Velocity: 1000 mm/s.

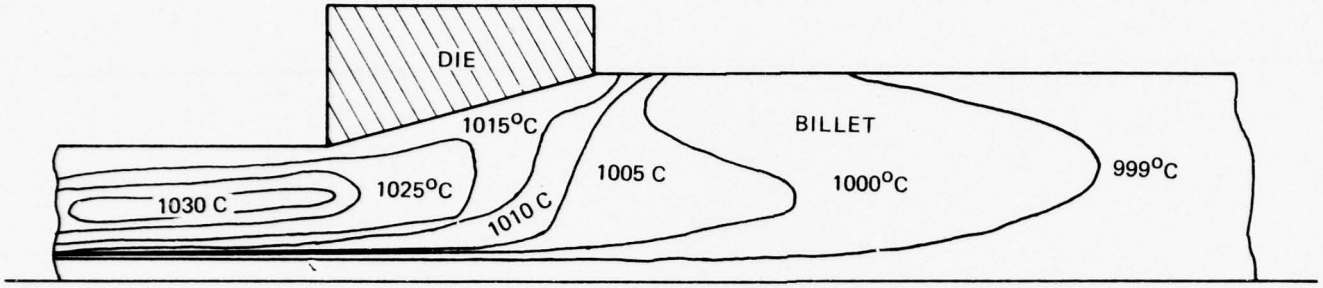

Figure 27. Temperature Distributions in Hot Drawing of Steel Shells Through a Conical Die 0.145 Seconds After Drawing Starts
(Billet Temperature = 1000°C, Tooling Temperature = 20° C) Speed: mm/sec

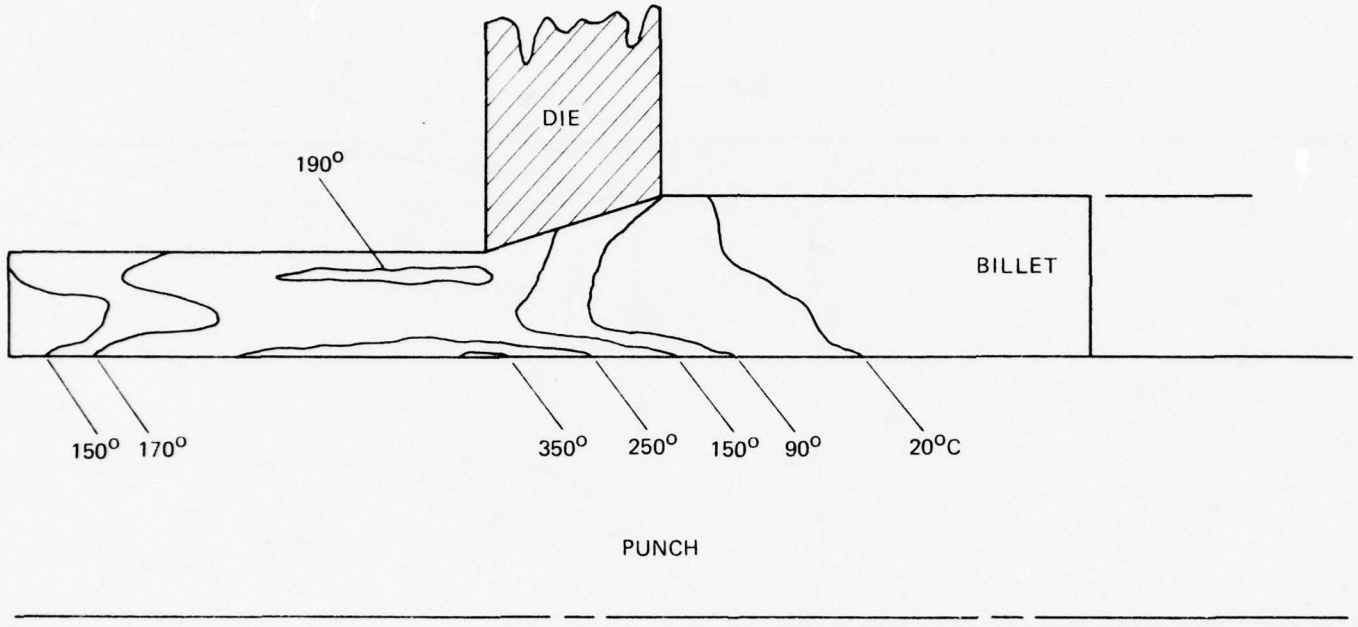

Figure 28. Temperature Distribution in Drawing of Steel Billet Through Various Dies. (Billet, Tooling Initial Temperature 20° C). Velocity: 200 mm/s.

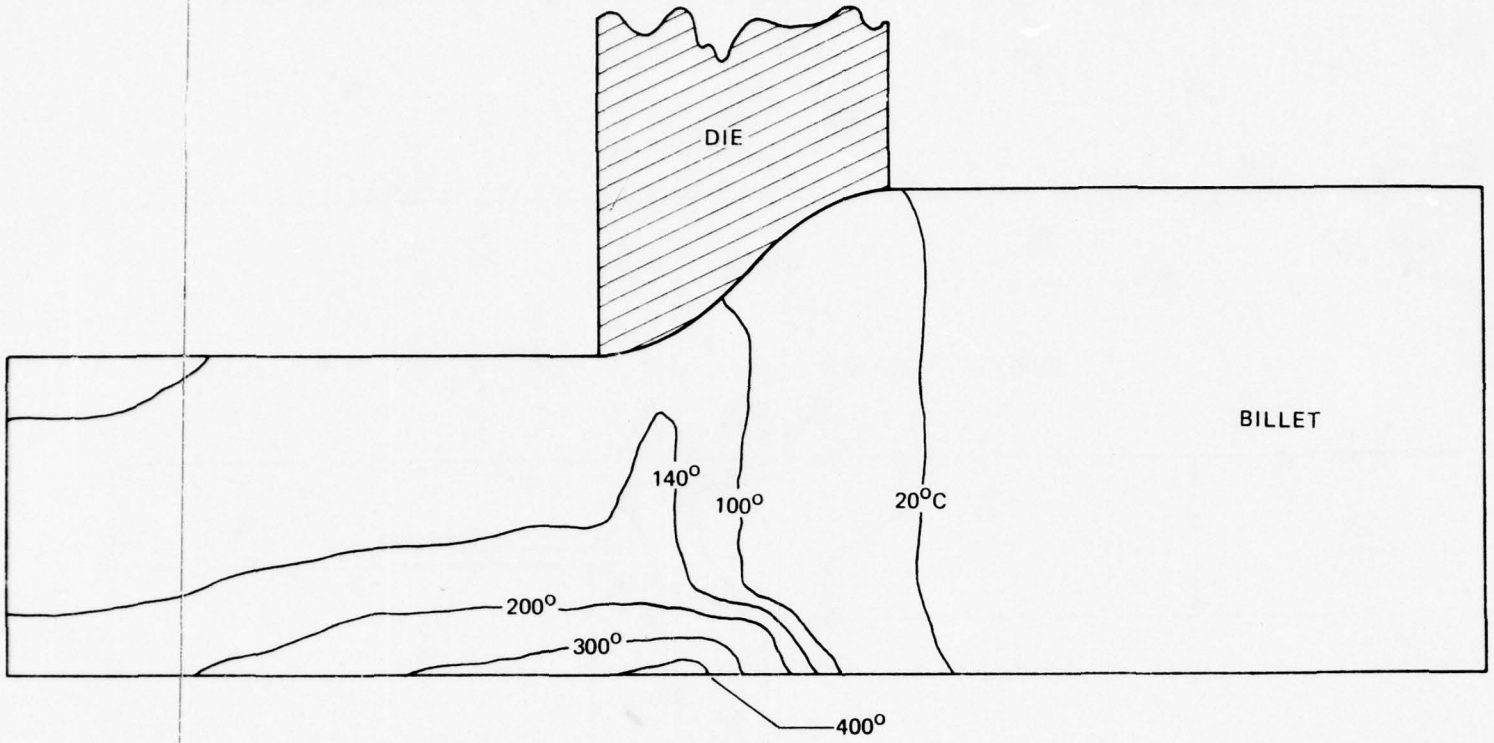

Figure 29. Temperature Distribution in Drawing of Steel Billet Through Various Dies. (Billet, Tooling Initial Temperature 20° C). Speed: 200 mm/sec.

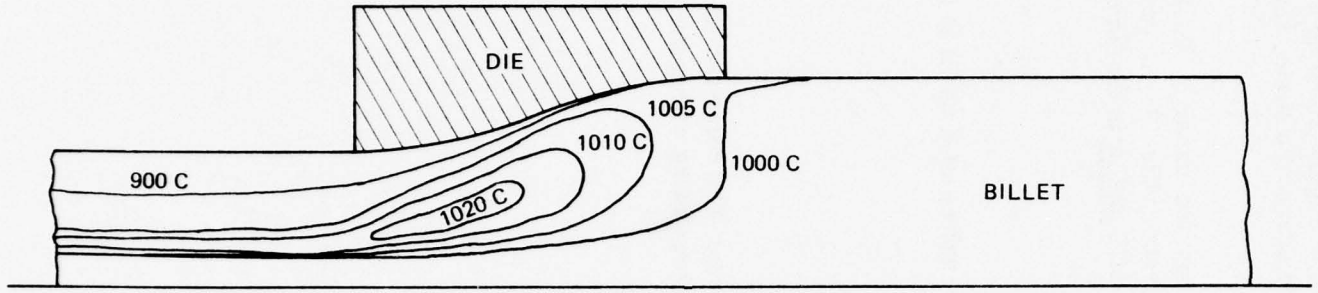

PUNCH

Figure 30. Temperature Distributions in Hot Drawing of Steel Shells Through a Double Curvature Die 0.145 Seconds After Drawing Starts (Billet Temperature = 1000° C. Tooling Temperature = 20° C). Speed: mm/sec

Figure 30 shows the hot drawing of the steel billet through optimal double curvature dies. The conditions used were identical to those of Figure 26 using a conventional die. As can be noted the temperature distributions are nearly the same, they differ only by about 10° C.

The data shown in Table 7 have been taken from the paper by T. Altan and F. W. Boulger in Trans. ASME, J. Engineering for Industry, Vol. 95, November 1975, pp 1009-1019. It should be noted that the values of C and m in the formula for hot working

$$\bar{\sigma} = C\ (\dot{\bar{\epsilon}})^m$$

are functions of the strain and temperature. The values of K and n in the formula for cold working

$$\bar{\sigma} = K\ (\bar{\epsilon})^n$$

are functions of the strain rate.

The data are stored in memory in tabular form. The computer automatically choses the correct values of C, m, K and n by interpolating within the table.

SUMMARY AND DISCUSSION

In this study mathematical models were developed and used to establish theoretical data for the design and optimization of single pass die rings. Two die rings were considered: (1) optimal curved dies, and (2) conventional tapered rings. The effects of temperature, punch speed, friction, heat transfer, and material were used in developing the data presented in the section entitled Simulation Results. The major conclusions and design guidelines for each of the two die types are given below. For clarity also given, were needed, is a specific figure or table number from the Simulation Results section. Also undertaken was a study to show the effect of heat transport on the drawing process. Conclusions are presented at the end of this section.

I. OPTIMAL CURVED DIES

1. The design of optimal, curved die profiles has been demonstrated theoretically. As shown in Figure 1, these dies are sigmoidal, that is doubly curved and streamlined. These profiles are formed from the blended radii of two circles. Optimal in the present context means that: for a specified reduction, shell metal and friction condition, this curved die profile, when compared to a conventional tapered die, is superior in that:

   a. Less energy is required from the press to form the drawn product.

   b. The residual strain distribution in the product wall, at the die exit, is more uniform through the wall thickness.

   The first factor, less energy used, indicates a potential cost savings by reducing plant power requirements. While the findings here are theoretical, an experimental study conducted by US Steel for drawing sheet and strip, indicated that using properly designed curved dies resulted in a 10% energy savings. The second factor, homogeneous strain distribution in the wall, indicates a reduced likelihood of failure by punch through. This would result in reduced scrap.

2. An additional consideration in the die design is the potential for product failure due to punch through of the moving mandrel. In this study a criterion to predict failure was postulated. It was assumed that when the specific draw stress exceeds unity, failure occurred. The specific draw stress was found to be dependent upon that temperaute, friction, mandrel speed and the stress-strain curve of the metal. (See Section IV on Failure Models for details and limitations).

3. Computer programs which perform the required design calculations have been developed. The programs have been made as user-oriented as possible. Input is punched on three cards, and consists of the steel being used, billet size and reduction desired. The optimal curved die profile is generated in about three minutes on the CDC 6500 at a cost of about $50. The program automatically prints out the: optimal die contour, press energy requirements, loads on the dies, loads on the shell, loads on the punch. A failure analysis and diagnosis of potential punch through is automatically performed.

4. As a result of this study it was possible to delineate those factors which do or do not effect the optimal die shape. It was found that:

   a. The temperature of the billet has no effect on the shape.

   b. The stress-strain curve of the billet has a small effect on shape (Figure 2).

   c. Friction conditions between die and product and product and punch have a small effect on shape (Figure 5).

   d. The velocity of the punch does not effect shape.

   e. The most significant factor effecting shape is the areal reduction (Figures 6-14).

5. A study to develop optimal die contours in drawing a 105 mm 1045 steel billet was performed. Figures 6-14 shown are the contours for reductions of 29%, 32%, 36%, 40%, 41%, 42%, 44%, 48% and 51%, respectively.

6. It was possible to delineate those factors which effect failure in optimal dies. It was found that:

   a. Temperature has a significant effect on raising the specific draw stress, which determines failure (Figure 2, Table 2). It was found that, at larger reductions, certain steels cannot sustain even a moderately hot draw. 1095 and 52100 steels at 750° C will fail in a 40% draw. These same steels will, in the cold (20° C) condition, probably sustain a cold draw without failure.

   b. Friction has a large effect on potential failure (Figure 3 and 4). It was established that reducing the friction between shell and die permits larger reductions. It was found, conversely, that increasing the friction between die and mandrel allows a larger reduction. This latter effect may be explained by noting that the force necessary to draw a shell is the sum of two parts: (a) the draw stress in the shell wall, caused by the action of the mandrel on the bottom of the shell and (b) the friction between the mandrel and shell. Thus, when the friction is increased, a greater part of the total load is carried by the mandrel, and the draw stress is lowered.

      It was also established that, regardless of friction, 40-41% is the largest possible reduction in a single pass, cold draw of a 105 mm projectile. Reductions beyond this point led to a specific draw stress much greater than one. It was also shown that the greater the reduction, the lower the strain homogeneity in the product wall.

II. CONVENTIONAL TAPERED DIES

1. Unlike the optimal curved dies, in which the shape is not known a priority but is determined as part of the problem, conventional dies have a fixed known geometry (Figure A-1). Thus, the computer program developed to accommodate the calculations was much simpler. Using this program, the effects of friction, temperature and mandrel speed were delineated.

2. In cold drawing regardless of the friction conditions between shell and die, an increasing die angle reduces the specific draw stress and hence avoids failure. Decreasing the shell-die friction enhances the process by lowering the liklihood of failure (Figure 15).

3. For any friction conditions in cold drawing, there is a minimum angle below which drawing is not possible (Figures 15 and 16).

4. Increasing the mandrel-shell friction in cold drawing decreases the specific draw stress and thus lowers the chance of failure. It should be noted that the same conclusion was drawn for curved dies, and has been discussed above.

5. Provided the two coefficients of friction are equal, hot drawing (up to 1000° C) is very similar to cold drawing. In this condition the punch velocity has no effect on drawability. The condition of $\mu_1 = \mu_2$ is not met, however, in practice.

6. When the coefficients of friction differ, even by a small amount, the draw stress is considerably reduced in hot drawing. An increased punch velocity will, it is anticipated, increase the liklihood of punch through.

7. As in cold drawing, increasing the die-shell friction lowers the draw stress.

III. HEAT TRANSPORT

A study to delineate the effects of heat transfer during the drawing of both optimal and conventional dies was performed. Both hot and initially cold billets were investigated. The following conclusions were reached:

1. In hot drawing (billet uniform initial temperature 1000° C) the temperature increase, due to the conversion of plastic work to thermal energy, is small, on the order of 30° C. The optimal curved die has a slightly lower maximum final temperature (1020° C) than the conventional die 1030°). It was concluded that this increase is insignificant in determining the product's degraded yield strength, and is not important to failure. (Figures 25-27 and 30).

2. In cold drawing (billet uniform initial temperature 20° C) the temperature increases is higher than in hot drawing - it is between 330° and 380° C. The curved die achieves a higher final temperature, 400° C, than does the tapered die, 350° C. These temperatures, at normal operating speeds, are not significant to failure.

With these facts in mind, the broad contributions which can result from math modeling studies include:

1. A method to predict the suitability of present equipment to future shell metals or configurations.
2. A method to predict the effects on present equipment by future changes in speed, temperature and lubricants.
3. An automated method for the preparation of technical data packages, and an aid in evaluating vendor's proposed draw presses and tooling configurations.
4. A reduction in scrap, and thus a subsequent increased economy of operation.

Those specific processing problem areas or data gaps which can be addressed by the results of this task include:

1. The effects of drawing of the higher mandrel speeds from a mechanical press.
2. The effects of temperature in a hot draw or reduced mechanical properties in the product wall.
3. The effects of friction between the punch and wall and between the wall and die rings.

RECOMMENDATIONS

Based on the results of this work, it is recommended that:

1. An experimental study by undertaken to confirm the optimality of the sigmoidal die rings theoretically designed in this report. Subject to such confirmation, these die rings should be made available for contractor use in shell manufacture.
2. The design procedures and associated software for shell drawing be made available to engineers involved in manufacturing process design.
3. The design procedures be extended to include tandem drawing with multiple die rings and a tapered mandrel.
4. The failure model will be modified to include plastic instability.
5. Additional work on hot drawing with conventional tapered dies with unequal friction coefficients be undertaken.
6. New modeling studies covering each step in shell manufacture be undertaken. These studies should include: nosing, billet separation, sizing, cabbage and pierce.

APPENDIX A

MATHEMATICAL MODELING

NOMENCLATURE

σ	axial stress
p	pressure
A	$\pi(r_2^2 - r_1^2)$, crossectional shell area
r_1	die radius, slab method
r_2	die radius, slab method
x	axial coordinate for generalized draw
$\mu 1^*$	coefficient friction between shell and mandrel
$\mu 2^*$	coefficient of friction between shell and die
P(x)	term
Q(x)	term
C	constant
R_o	radius
t_o	thickness
t_1	thickness
r_o	radius
α	die semi-angle
B	constant
R_1	radius, optimal curved die
R_2	radius, optimal curved due
$\bar{\epsilon}$	effective plastic strain
$\dot{\bar{\epsilon}}$	effective plastic strain rate
Z	axial coordinate for a tapered die
h	thickness for a tapered die
Z_a	axial position

*Explanation next page

Z_b axial position

t time

m_1 friction factor between die and shell

m_2 friction factor between shell and mandrel

---

*In the computer program SHELL friction is accounted for through the assumption of Coulomb's Law,

$$\frac{\text{tangential shear stress}}{\text{normal pressure}} = \frac{\tau}{p} = \mu$$

where μ is the coefficient of friction, which is taken as constant for a given die and shell.

In the programs CDVEL, SDVEL and SDTEM another expression for friction is used. It is assumed that

$$\frac{\text{tangential shear stress}}{\frac{1}{\sqrt{3}}\text{ yield strength of the shell}} = \frac{\tau}{\sigma_o/\sqrt{3}} = m$$

where m is the friction factor. This assumption is related to the von Mises yield criterion.

I. BACKGROUND/RATIONALE

Traditionally, the hot or cold drawing of shell has been carried out in hydraulic presses at moderate speeds up to 300 inches/min. Recently, presses which can draw at speeds beyond 2000 inches/min have been under consideration. The die and process design experience is largely regulated to lower speed machines. When new processing techniques and higher speeds are introduced, previous tooling experience alone is not sufficient to design the drawing process adequately. For example, when the drawing speed is increased 5 to 10 times over conventional speeds, it is necessary to utilize quantitative engineering analysis in order to predict under which conditions failure such as punch-through or wall-tearing could occur. This problem is typical of the interaction of temperature and strain rate in reducing strength at high processing speeds. Two objectives of this task, then are to provide models which can predict potential failure, and establish optimum combinations of the processing variables. The mathematical techniques required to meet these objectives are discussed below.

A review of the technical literature on the modeling of the shell drawing process indicates that, basically, the following three methods of attack have been applied to the mathematical study of the process: (a) the "Slab" or "Sachs" Method, (b) the "Method of Characteristics" or the "Slipline Analysis", and (c) "The Upper Bound" or "Minimum Energy" Method.

Using the slab method, Sachs[2] and his coworkers conducted the first mathematical analysis of the shell drawing process. Their study treated the process as a plane-strain problem and it was based on three main assumptions: (1) the deformation was a simple uniform (uni-axial) extension, (2) the principal stress directions were everywhere perpendicular and parallel to the punch surface, and (3) the plastic region extended between the two transverse planes containing the circles of contact of shell and die at entry and exit. With these assumptions, Sachs et al., [2] were able to derive and graphically solve the equilibrium equations for straight as well as curved dies. He also crudely introduced the effect of strain-hardening and of the strain-rate dependency of the shell material. Thus, Sachs' plane-strain analysis allows one to determine, within these approximations, the effect of process variables upon the draw force and upon the drawing limits in drawing very thin-walled shells. However, this analysis is not adequate for drawing of medium or thickwalled shells (artillery shells) and it does not include the thermal effects, i.e., heat generation and heat transfer, which are important aspects of the deformation process at higher speeds.

The slipline analysis assumes a rigid-perfectly plastic material. This method has been originally applied by Hill[3] to the solution of plane-strain shell drawing through conical dies. Similar studies have also been conducted for curved dies by Green,[4] Richmond and Devenpeck[5, 6, 7] and Sowerby, et al.,[8]. Recently, the slipline analysis has been extended to study axisymmetric extrusion and drawing operations by Richmond. Although the slipline analysis is among the most rigorous methods for investigating metal forming problems, it essentially neglects strain-hardening effects, strain-rate effects, as well as thermal phenomena in the deforming material. Consequently, its application to optimizing actual shell and cartridge drawing operations

requires modification. The outstanding advantage of this method is that the stress field is very accurately determined. Failures, such as cracking or central burst, depend on an accurate estimate of the state of stress for their prediction. Thus, this technique is required for examining failure modes. Progress utilizing this technique is presented in this report.

The upper-bound method describes the metal flow in the shell drawing operation by considering an admissible velocity field that satisfies the incompressibility, continuity, and the velocity boundary conditions. Based on this velocity field, the deformation, the shear (if velocity discontinuities are present), and the friction energies are computed to give the total forming energy and also the forming load. Based on limit theorems, (10) this calculated forming load represents an upper-bound to the actual forming load. Often, the velocity field considered includes one or more free parameters that are to be determined by minimizing the total forming energy with respect to those parameters. Thus, the determined values of the parameters enable a better upper-bound velocity field to be found.

Most of the upper-bound solutions available for processing of tubular products have been developed for extrusion. However, because of geometrical and fundamental similarities in metal flow, these analyses can also be applied, with appropriate modifications, to the shell-drawing process. A radial velocity field for tube extrusion through conical dies was derived by Avitzur[11] and also applied to practical extrusion studies by DePierre.[12] Chen and Ling[13] also utilized the upper-bound approach extensively to obtain solutions to axisymmetric extrusion problems with various curved dies. Chang and Choi[14] conducted similar studies on the extrusion of tubes through conical and curved dies. Mehta, et al.,[15] developed a unique superposition technique to develop a velocity field without discontinuities in analyzing the tube extrusion through conical dies.

The upper-bound solutions, discussed above, assumed that the material was rigid-perfectly plastic. It is possible to introduce, with some difficulty, the strain-hardening and strain-rate effects into these solutions. However, with the exception of Mehta's solution, all other upper-bound analyses include discontinuities in their velocity fields. Therefore, these discontinuities result in artificial and unrealistic sources of heat generation when a thermal analysis of the drawing process is conducted. Consequently, the existing upper-bound studies required significant improvement in order to develop a sound mathematical model of the shell drawing process. That modification is given in this report and in greater detail in the Battelle report.

Although the influence of temperature and speed in shell drawing processes is well known, a realistic thermal analysis of the shell drawing operation does not exist. However, several attempts have been made in the past to predict, at least approximately, the temperature distributions in some kinematically steady-state deformation processes, such as axisymmetric extrusion and drawing of rod and wire. Most recently, with the wide use of digital computers, numerical methods have been more widely introduced. These methods are capable of describing the complex physical

phenomena involved in extrusion or drawing without the many simplifying assumptions as it is the case in using analytical methods of solution.

In plane-strain extrusion, Bishop[16] developed the principles of a numerical method by separating the complex problem of heat generation, conduction and transportation into two parts. Thus, the heat generation and transportation are regarded as occurring instantaneously, followed by an interval in which conduction takes place as for a stationary medium. Altan and Kobayashi[17] developed this method further and developed computer programs for determining temperature distributions in extrusion of round bars by using experimentally obtained data on metal flow. Altan's[17, 18, 19, 20] studies have been further expanded by using an axisymmetric upper-bound velocity field without discontinuities to calculate the heat generation and the heat transport during deformation. This work has been further applied to predicting temperatures in extrusion of rods and in drawing of rod and wire.

Based on the relative advantages and disadvantages of the available methods discussed above, it was decided to simultaneously:

1. Develop a very general upper-bound approach which could handle high and low forming rates and temperature generation.
2. Expand the slip line (method of characteristics) techniques to include high forming rates.
3. Expand the Sachs' or Slab Method for failure prediction.

The first effort was carried out under contract with Battelle. The second was performed in-house at Frankford Arsenal. The third was a joint Battelle/Frankford Arsenal effort.

II. THEORY

In order to make the present report complete and self-contained, the basic theoretical considerations of all methods used in developing the various math models are sketched here. For details concerning the upper bound method, together with the associated computer programs reference to the Battelle report is made.

II A. THE UPPER BOUND METHOD

The basis of the method, due originally to Prager[17], and modified by Altan[17] and his associates is essentially as follows:

1. A velocity for the flowing metal is guessed. The "best" guess is given by adhering to the following principals:
   a. The flow must be incompressible.
   b. The flow must be continuous.
   c. The flow must satisfy the velocity boundary conditions.

2. Based on the velocity field generated above, the deformation (strain rates, velocity gradients, etc), the shear energy (if velocity discontinuities were allowed), and friction energies are calculated. Based on the limit theorems of plasticity[17] the forming load is higher than the actual load and it, thereby, represents an upper bound to the actual forming load. It also follows that the lower the upper bound load, the better prediction of metal flow. One way of insuring a "best" (smallest) upper bound is to use the calculus of variations. Unknown parameters are introduced into the energy function and the entire function minimized according to the rules of the calculus of variations.

As an example and to develop the theory, the case of drawing through conical dies is presented. As shown in Figure A-1 a tubular billet of outer radius $1 + r_o$ and an inner radius, r_o, is drawn through a conical die of half angle α, to a final wall thickness b, using a cylindrical punch of radius r_o.

A basic velocity field is assumed by a plastically deforming region (region 2 in Figure A-1) bounded by the velocity discontinuity surfaces ACQ and BDP. The flow lines in the regions before and after the deformation region are also assumed to be straight lines, parallel to the axis of drawing. The radial distances R_k and r_k, of the flow lines from the surface of the punch are related to each other because of incompressibility. Thus:

$$r_k = - r_o + \sqrt{r_o^2 + V_e (R_k^2 + 2 R_k r_o)}$$

$$\text{and} \quad R_k = - r_o + \sqrt{r_o^2 + (r_k^2 + 2 r_k r_o)/V_e}, \tag{1}$$

where V_e is the velocity at the entrance or billet velocity. Unlike tube extrusion, in shell drawing, the process speed is controlled by the punch velocity, which is the same as the product velocity. The billet velocity, V_e for unit punch velocity, V_f, is given by

$$V_e = \frac{b\,(b + 2 r_o)}{1 + 2 r_o} \tag{2}$$

Let the flow lines in region 2, Figure A-1, be represented by the equation

$$z = \left(E + \frac{F}{r_k} + \beta r_k \right) \left(r - r_o \right) + G r_k + H , \tag{3}$$

where E, F, G, H and β are to be determined from the boundary conditions. Omitting the details, which are given in Reference 1. The net result is

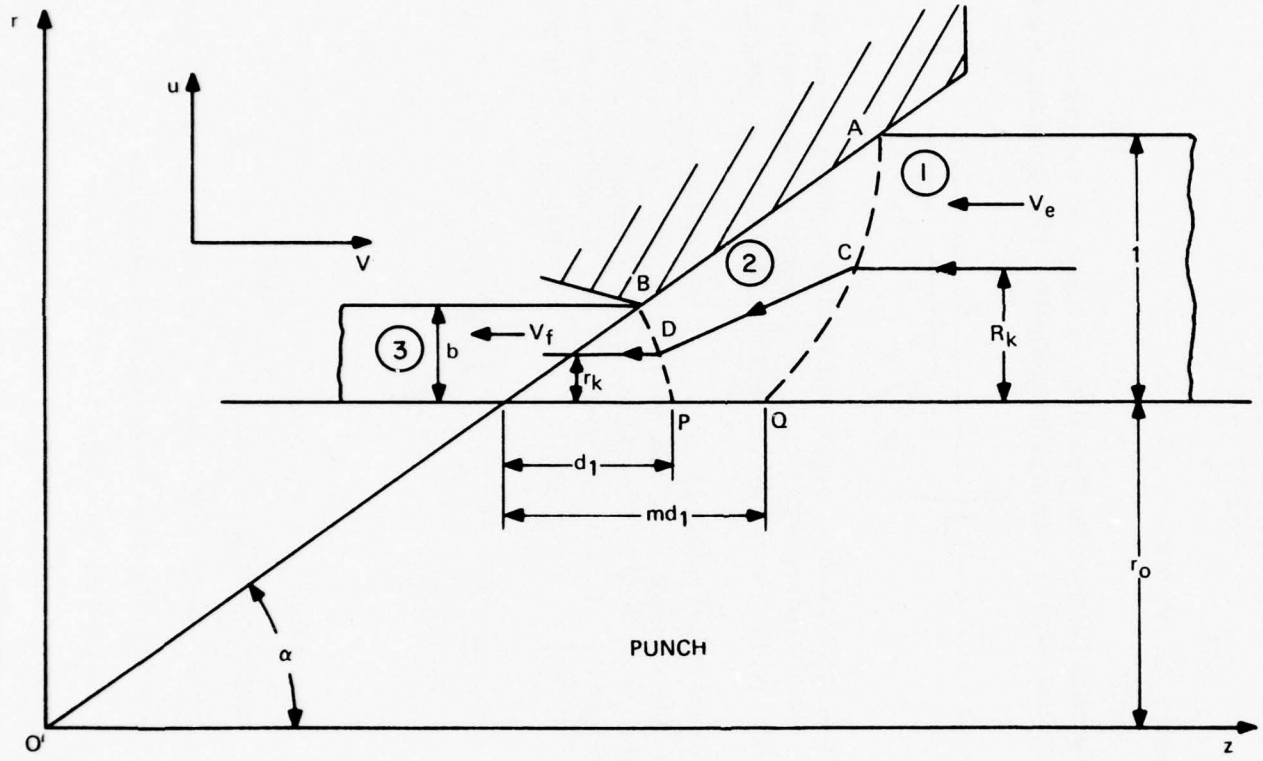

Figure A-1. Geometry of Axisymmetric Metal Deformation in Shell Drawing

$$\text{in region (1)}, \quad r_k = -r_o + \sqrt{r_o^2 + \left(r^2 - r_o^2\right) V_e}, \tag{4.a}$$

$$\text{in region (2)}, \quad r_k = \frac{d_1}{\frac{z - r\cot\alpha}{r - r_o} + \frac{d_1}{b}}, \tag{4.b}$$

$$\text{and in region (3)}, \quad r_k = r - r_o, \tag{4.c}$$

The intersection between the flow lines in region (2) and region (1) determines the equation for the line ACQ of velocity discontinuity. This equation is given by

$$z = r\cot\alpha + \frac{d_1}{b}(r - r_o)\left[\frac{b}{-r_o + \sqrt{r_o^2 + (r^2 - r_o^2) V_e}} - 1\right] \tag{4.d}$$

The parameter d_1 in Equation 4, separating the flow regions, is not as yet determined by imposition at the boundary conditions. In the spirit of the calculus of variations the parameter d_1 will be determined by the condition that a certain integral be a minimum.

For a given extrusion ratio, die angle, and friction factor, the actual external work rate is a function of the only unknown parameter d_1 of Figure A-1. The unknown parameter d_1 can be derived for the determination of an optimum velocity field, using the upper-bound theory. For this purpose, d_1 must be such that the rate of energy $\dot{E}$, consumed in the process, is a minimum. The energy rate, $\dot{E}$, is given by

$$\dot{E}(d_1) = \bar{\sigma}\cdot\left[\frac{2}{\sqrt{3}}\int_V \sqrt{\frac{1}{2}\,\dot{\epsilon}_{ij}\,\dot{\epsilon}_{ij}}\,dV + \int_{S_1} f_1 \cdot \Delta V_1 dS_1 - \int_{S_2} f_2 \cdot \Delta V_2 dS_2\right], \tag{5}$$

where

$\bar{\sigma}$ = flow stress of shell material

V = volume of the deformation zone

f_1 = friction factor at the shell-die interface, $(0 \leq f_1 \leq 0.577)$

ΔV_1 = velocity difference at the shell-die interface

S_1 = shell-die interface area

f_2 = friction factor at the shell-punch interface, $(0 \leq f_2 \leq 0.577)$

ΔV_2 = velocity difference at the shell-punch interface

S_2 = shell-punch interface area excluding the product

ϵ_{ij} = strain rates.

In order to evaluate Equation 5 we need to substitute expressions for the velocities and strain rates.

For incompressible materials, the velocity fields in steady-state axisymmetric plastic deformation processes can be defined by introducing a flow function ψ, such that

$$u = \frac{1}{r}\frac{\partial \psi}{\partial z} \text{ and } v = -\frac{1}{r}\frac{\partial \psi}{\partial r} \tag{6}$$

where u and v are the velocity components in the radial (r-) and the axial (z-) directions, respectively, and $\psi = \psi(r, z)$. The flow lines are then given by,

$$\psi = C_k \tag{7}$$

where C_k is a constant along the k-th flow line and proportional to the rate of volume flowing through the flow layer. The volume rate flowing through a flow layer bounded by the k-th flow line is proportional to $\frac{1}{2} V_e\, r_k\, (r_k + 2\, r_o)$ where r_k, in various regions, is given by Equation 1. The flow function ψ, of the basic flow pattern, is expressed in the form of

$$\psi = \frac{1}{2}\, V_e\, r_k\, (r_k + 2\, r_o). \tag{8}$$

The velocity components are then calculated according to

$$u = \frac{1}{r}\frac{\partial \psi}{\partial z} = \frac{V_e}{r}(r_k + r_o)\frac{\partial r_k}{\partial z} \tag{9.a}$$

$$V = -\frac{1}{r}\frac{\partial \psi}{\partial r} = \frac{V_e}{r}(r_k + r_o)\frac{\partial r_k}{\partial r} \tag{9.b}$$

The velocity field given by Equation 8 contains velocity discontinuities. A continuous velocity field can be obtained by superimposing several basic flow patterns, each of which is given by a pair of velocity discontinuity lines as shown in Figure A-1. The details are given in Reference 1. The strain rates may be in turn calculated from

$$\dot{\epsilon}_r = \frac{\partial u}{\partial r} = \frac{\partial}{\partial r}\left[\frac{1}{r}\frac{\partial \psi}{\partial z}\right] \tag{10.a}$$

$$\dot{\epsilon}_\theta = \frac{u}{r} = \frac{1}{r^2}\frac{\partial \psi}{\partial z} \tag{10.b}$$

$$\dot{\epsilon}_z = \frac{\partial v}{\partial z} - \frac{1}{r}\frac{\partial^2 \psi}{\partial r \partial z} \tag{10.c}$$

$$\dot{\epsilon}_r = \frac{1}{2}\left(\frac{\partial u}{\partial z} + \frac{\partial v}{\partial r}\right) = \frac{1}{2}\left[\frac{1}{r}\frac{\partial^2 \psi}{\partial z^2} \quad \frac{\partial}{\partial r}\left(\frac{1}{r}\frac{\partial \psi}{\partial r}\right)\right] \tag{10.d}$$

Once the optimum value of d_1 corresponding to the minimum energy rate, $\dot{E}$, is known, then the best member of the selected class of velocity fields is given by Equation 9. These calculations, including the minimization of $\dot{E}$ (d_1), have been programmed for use at Frankford Arsenal on a CDC 6500/6600 computer.

II B. PERTURBATION APPROACH

The objectives of this portion of the work were to develop mathematical methods capable of providing: (a) a detailed stress analysis, (b) a failure analysis of drawing, and (c) solutions to problems not handled by the upper bound method

In order to meet the above objectives the work has been divided into three sub-tasks. A brief description of these sub-tasks follows.

Sub-Task 1. Evaluation of Existing Perturbation Methods

This sub-task consisted of exploring perturbation techniques which have proven successful in other areas of deformation mechanics. The possibility of application of this method to plasticity, and to metalforming problems in general, was found to be excellent. Lin[21] and Fox[22] developed the technique for compressible fluid mechanics. Richmond[23] later noted the similarity between the fluid mechanics case and plasticity. It was apparent that this technique is capable of giving a detailed stress analysis of the deforming product. This capability is important in determining failure modes in drawing. This, of course, cannot be done using the upper bound method.

A second perturbation method, suggested by, Onat[24] includes the effects of work-hardening and flow stability on plasticity. A careful examination of these two precedures was completed, and the two techniques were persued. Details of this investigation are presented below.

Sub-Task 2. Adaptation of Lin's Method for Metal-Forming Process

This model is applicable to determining residual stress and strain during processing. The model is idealized in that: the product metal is cold, non-work-hardening and experiences no friction between the die-shell and mandrel-shell interfaces.

Sub-Task 3. Adaptation of Onat's Method for the Shell Forming Process

This model is used in conjunction with Lin's method, to study the states of stress, strain and velocity in the product. The model is less idealized than that of sub-Task 2 in that work-hardening can be considered.

The basis of the Lin method is presented in References 21, 22. The concept is as follows:

1. The partial differential equations governing the plastic flow are written down in terms of the characteristics or slip lines. If the equations are not hyperbolic the method does not apply.

2. The independent variables are the characteristics of the original field equations. The dependent variables are the stresses, velocities and Eulerian positions.

These dependent variables expanded in a series involving a small (perturbation) parameter ϵ, and each term in the series is treated as a function of the characteristic parameters.

In order to illustrate the method, the problem of tubular drawing through dies is sketched below. The notation is essentially that of Reference 23.

Under the assumption that the deforming material is rigid-perfectly plastic, the characteristic equations are

$$(P + \phi), \alpha + (Z \pm r), \alpha / 2r = 0 \tag{11.a}$$

$$(P - \phi), \beta - (Z \mp r), \beta / 2r = 0 \tag{11.b}$$

$$Z, \alpha = \tan \phi \; r, \alpha \tag{11.c}$$

$$Z, \beta = \cot \phi \; r, \beta \tag{11.d}$$

$$U, \alpha - V\phi, \alpha + (U_r, \alpha - V_z, \alpha)/2r = 0 \tag{11.e}$$

$$V, \beta + U\phi, \beta + (U_z, \beta + V_r, \beta)/2r = 0 \tag{11.f}$$

In Equation 11: r and z are cylindrical coordinates, α and β are the characteristic parameters, and P, ϕ, u and v are related to the usual stress and velocity components by

$$P = -(\sigma_r + \sigma_z)/4k \tag{12.a}$$

$$2\phi = \tan^{-1}[(\sigma_z - \sigma_r)/2\tau_{rz}] \tag{12.b}$$

$$U = u \cos \phi + v \sin \phi \tag{12.c}$$

$$V = -u \sin \phi + v \cos \phi \tag{12.d}$$

The following assumptions are now made:

$$P = P^o + \epsilon P' + \epsilon^2 P'' + \ldots \tag{13.a}$$

$$\phi = \phi^o + \epsilon \phi' + \epsilon^2 \phi'' + \ldots \tag{13.b}$$

$$r = r^o + \epsilon r' + \epsilon^2 Z'' + \ldots \tag{13.c}$$

$$z = z^o + \epsilon z' + \epsilon^2 Z'' + \ldots \tag{13.d}$$

where each of the P, ϕ, r, z are functions of the true characteristics α and β.

Equation 13 is now introduced into Equation 11 and like order terms collected. The zeroth order perturbed counterpart of Equation 11 a-d is thus:

$$(\cos \phi^{o})\, Z^{o}, \alpha = (\sin \phi^{o})\, r^{o}, \alpha \tag{14.a}$$

$$(P^{o} + \phi^{o}), \alpha = 0 \tag{14.b}$$

$$(P^{o} - \phi^{o}), \beta = 0 \tag{14.c}$$

$$(\sin \phi^{o})\, Z^{o}, \beta = -(\cos \phi^{o})\, r^{o}, \beta \tag{14.d}$$

The first and higher order perturbed quantities have not as yet been derived.

By examining Equation 14, it can be seen that they represent a simpler system of equations than does Equation 11. While Equation 14 is not linear the terms involving 1/r from Equation 11 do not appear. It is anticipated that Equation 14 and the higher order perturbed equations will lead to a solvable system of equations.

II C. THE ONAT PERTURBATION METHOD

The basis of the method is presented in Reference (24). A derivation of the fundamental equations is presented below.

For a rigid-work hardening body the stress-strain relations are

$$\dot{\epsilon}_{ij} = F\, S_{ij}\, \dot{J}_2, \text{ if } J_2 \geq k^2,\ \dot{J}_2 > 0 \tag{15.a}$$

$$\dot{\epsilon}_{ij} = 0 \quad , \text{ if } J_2 < k^2,\ \dot{J}_2 < 0 \tag{15.b}$$

where

σ_{ij} = stress tensor

$\dot{\epsilon}_{ij}$ = strain rate tensor

S_{ij} = stress deviator $= \sigma_{ij} - 1/3\, \sigma_{pp}\, S_{ij}$

J_2 = $1/2\, S_{ij}\, S_{ij}$

$\dot{J}_2$ = material derivative of J_2

k = yield stress in shear

It is assumed that the velocities, stress and strain rates, referred to conventional Cartesian coordinates, X_i, can be expanded in a time series as

$$V_i(a_p, t) = V_i^{\circ}(a_p) + t\,\gamma_i(a_p) + \ldots + \tag{16.a}$$

$$\sigma_{ij}(a_p, t) = \sigma_{ij}^{\circ}(a_p) + t\,\sigma'_{ij}(a_p) + \ldots + \tag{16.b}$$

$$\epsilon_{ij}(a_p, t) = \epsilon_{ij}^{\circ}(a_p) + t\,\epsilon'_{ij}(a_p) + \ldots + \tag{16.c}$$

where

γ_i = Lagrangian acceleration

σ'_{ij} = rate of stress

ϵ'_{ij} = velocity strain (strain rate)

a_p = Lagrangian coordinates

and the quantities with a superscript "0" are evaluated at $t = 0$, the yield point state. These satisfy the following equilibrium, yield condition and kinematic quantities

$$\begin{aligned} \overline{\sigma}_{ij}^{\,o}{}_{,j} &= 0 \\ J_2^{\,o} &= 1/2\, S_{ij}^{\,o} S_{ij}^{\,o} = k^2 \\ \epsilon_{ij}^{\,o} &= 1/2\,(V_{i,j}^{\,o} + V_{j,i}^{\,o}) = F(J_o)\, S_{ij}^{\,o}\, [\dot{J}_2]_{t=0} \end{aligned} \tag{17}$$

The first order quantities satisfy

$$\epsilon_{ij} = 1/2\,(\gamma_{i,j} + \gamma_{j,i}) - 1/2\,(V_{i,p}^{\,o} V_{p,j}^{\,o} + V_{j,p}^{\,o} V_{p,i}) \tag{18}$$

$$\sigma'_{ij,j} - V_{p,j}^{\,o}\, \sigma_{ij,p}^{\,o} = 0 \tag{19}$$

$$2\, S_{ij}^{\,o} S'_{ij} = \frac{\sigma_{ij}^{\,o}\, \epsilon_{ij}^{\,o}}{F(J_2^{\,o}) \cdot J_2^{\,o}} \tag{20}$$

where

$$S'_{ij} = \left(\sigma'_{ij} - \frac{1}{3}\, S_{ij}\, \sigma'_{pp}\right); \quad \left[\frac{dJ_2}{dt}\right]_{t=0} = S_{ij}^{\,o} S'_{ij} \tag{21}$$

$$\epsilon'_{ij} S_{pq}^{o} + \epsilon_{ij}^{o} S'_{pq} - \epsilon_{pq}^{o} S'_{ij} - \epsilon'_{pq} S_{ij}^{o} = 0 \ldots , \quad (22)$$

Equations 18, 19, 29 and 22 govern the first order quantities.

A comparison of Upper Bound and Perturbation methods is shown in Tables A-1 and A-2.

Table A-1. The Range of Application for Each Math Model

	Metalworking Application			
Math Model	Stress Analysis	Forming Loads	Failure (Punch Through)	Optimum Die Design
Upper Bound	No	Yes	Limited	Yes
Lin Perturbation	Yes	Limited	Limited	No
Onat Perturbation	Yes	Limited	Yes	No

Table A-2. The Range of Metalworking Parameters for Each Math Model

	Metalworking Parameter			
Math Model	Elevated Temperature	Strain Hardening	Strain Rate	Friction*
Upper Bound	Yes	Yes	Yes	Yes
Lin Perturbation	No	No	No	Yes
Onat Perturbation	No	Yes	No	?**

* Between tooling and workpiece.

** Theory is insufficiently developed to comment.

II.D SLAB METHOD

In the preceding sections, the upper bound method has been used to analyze drawing. As mentioned there, the upper bound method suffers from the disadvantage that the stress distributions calculated are not accurate. Failure, if it occurs, is due to tearing of the shell wall. Tearing in turn is related to an excessive axial stress in the drawn product. Thus, for purposes of design it is necessary to have an accurate estimate of the stress in the product wall. The purpose of this section is to present an analysis which meets this requirement.

Since it has been established earlier in this report that optimal dies are dies which are curved rather than conical, the stress analysis formulae given here are very general and are applicable to any curved or conical die. Also, since in practice the mandrel is tapered or curved this also is considered.

Figure A-2 shows a diagram of the shell drawing process. Both the die contour and mandrel contour are allowed to be specified functions of the axial coordinate, x. Since the shell geometry has cylindrical symmetry about the x-axis, only the two radii, r_1 and r_2, are required to completely specify the shape. The forces or stresses acting on the element (exploded view) are: the stress, σ_x; the normal pressure, p, and the frictional forces $\mu_1 p$ and $\mu_2 p$. Equating these forces to zero results in the following equation of equilibrium:

$$\sigma A + \frac{d}{dx}(\sigma A)\,dx - \sigma A - p r_2\, dr_2\, 2\pi + p r_1\, dr_1\, 2\pi + \mu_2 p\, 2 r_2\, dx\, 2\pi - \mu_1 p_1 r_1\, dx\, 2\pi = 0 \tag{23}$$

Simplifying and noting that

$$A = \pi (r_2^2 - r_1^2) \tag{24}$$

it follows from (23) that

$$\frac{d}{dx}\left[\sigma(r_2^2 - r_1^2)\right] + 2p\left[r_2 \frac{dr_2}{dx} - r_1 \frac{dr_1}{dx}\right] + 2p\left[-r_1\mu_1 + r_2\mu_2\right] = 0 \tag{25}$$

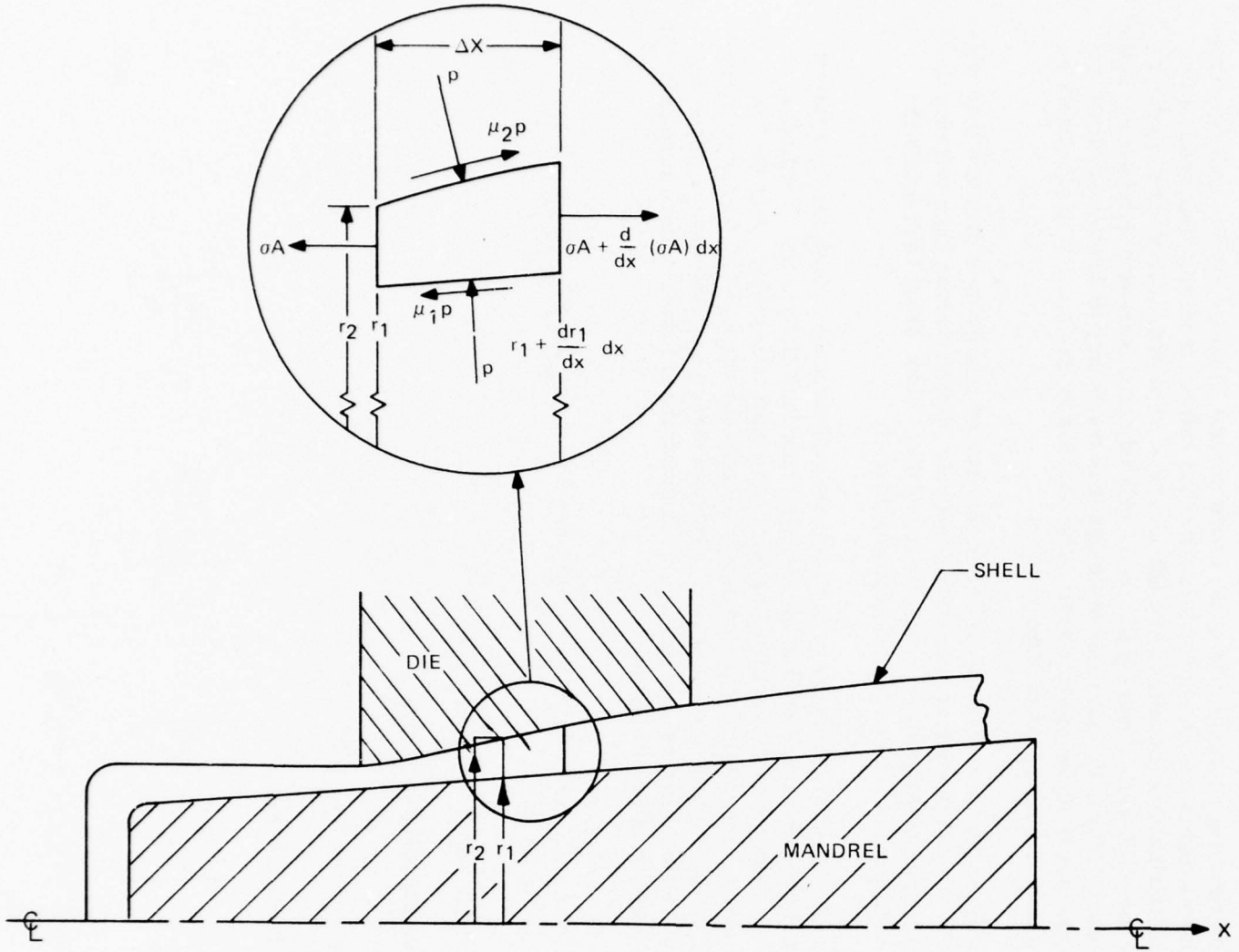

Figure A-2. Forces Acting on an Element in Drawing with Curved Die and Curved Mandrel

According to Sachs [2.a], the yield condition is

$$p + \sigma = \frac{2}{\sqrt{3}} \bar{\sigma} \tag{26}$$

where $\bar{\sigma}$ is the yield strength of the metal. Eliminating p from Equation 25 by using 26 gives

$$\frac{dp}{dx} + P(x)\sigma = Q(x) \tag{27}$$

where

$$P(x) \equiv -\left[\frac{2(\mu_2 r_2 - \mu_1 r_1}{(r_2^2 - r_1^2)}\right]$$

$$Q(x) \equiv -\frac{2\left[(r_2 r_2' - r_1 r_1') + (\mu_2 r_2 - \mu_1 r_1)\right]}{(r_2^2 - r_1^2)} \tag{28}$$

Equation 27 is a first order linear differential equation with variable coefficients for the unknown stress $\sigma(x)$. The solution of this equation is

$$\sigma(x) = C \exp\left(-\int p\, dx\right) + \left[\exp\left(-\int p dx\right)\right] \cdot \left[\exp\left(-\int p dx\right) \cdot Q dx\right] \tag{29}$$

where C is a constant of integration. This constant may be found by noting that at X = 0, at the entrance to the die, the applied force is zero. Thus

$$\sigma(0) = 0 \tag{30}$$

is the required condition.

The above, Equation 24, is valid only for a single die ring. In the case of two or more rings (tandem drawing) this would be replaced by the conditions that: (a) the stress is zero going into the first die and (b) the stress must be continuous upon entry into the second die. This work has not as yet been carried out.

In general, although the solution given by Equation 24 is in closed form, the actual integration is difficult analytically except under certain special cases. In general, numerical integration may be required. For the conical die the integration is simple and is given in the next section.

The failure criterion is given by Sachs as follows: When the total drawing stress (total drawing load/shell area at die exit) exceeds $2/\sqrt{3}$ times the yield strength (as measured at the exit), then tensile wall failure occurs. The total drawing stress is the sum of all the axial forces acting on the shell and on the mandrel divided by shell cross-sectional area at the exit. This is not to be confused with the "actual stress" σ, given in the above formulas. The drawing stress is actually a fictious quantity which is useful in defining the drawing limits or failure in a proposed process.

In this report the special case of a conventional conical was treated. In order to accomplish this the above equations are reduced to the equations for a conical die of semi-angle α and a straight mandrel. Thus referring to Figure A-3, the inner radius, r_1, is a constant, r_o, or

$$r_1 = r_0 \tag{31}$$

and the radius r_2 is a linear function of Z

$$r_2 = \left(\frac{R_1 - R_0}{Z_a - Z_b}\right) Z + R_1 - \left(\frac{R_1 - R_0}{Z_a - Z_b}\right) Z_a \tag{32}$$

Using Equations 31 and 32 in the previous equations results in a stress distribution

$$\sigma(Z) = \left(\frac{1 + B}{B}\right) \frac{2}{\sqrt{3}} \sigma \left[1 - \left(\frac{r_2 - r_0}{R_0 - r_0} \right)^B \right] \tag{33}$$

where

$$B = (\mu_2 - \mu_1)/\tan\alpha \tag{34}$$

At the exit where $r_2 = R_1$ the actual stress is

$$\sigma\Big|_{Z_a} = \left(\frac{1 + B}{B}\right) \left[1 - \left(\frac{R_1 - r_0}{R_0 - r_0} \right)^B \right] \tag{35}$$

The total draw force consists of two parts, F_1 and F_2: where F_1 is the resultant of the tensile stresses acting on the shell at the exit, and F_2 is the force on the mandrel

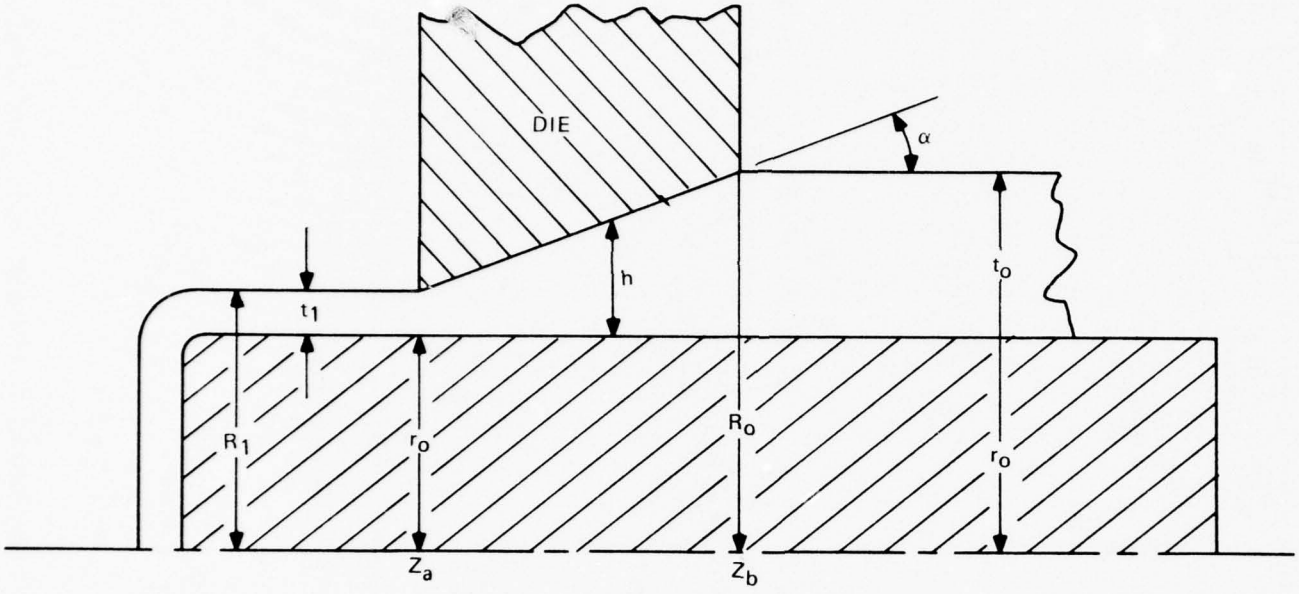

Figure A-3. Geometry of a Tapered Die with a Straight Mandrel

due to the components of normal pressure and friction acting in the axial direction. From Equation

$$F_1 = \pi (R_1^2 - r_0^2) \frac{2\bar{\sigma}}{\sqrt{3}} \left(\frac{1+B}{B}\right) \left[1 - \left(\frac{R_1 - r_o}{R_o - r_o}\right) B\right] \tag{36}$$

$$F_2 = 2\pi r_0 / \mu_2 \int_{Z_a}^{Z_b} p\,dz \tag{37}$$

since

$$dz = dh/\tan\alpha \tag{38}$$

and

$$p = \frac{2}{\sqrt{3}} \bar{\sigma} - \sigma \tag{39}$$

$$F_2 = 2\pi r_0 \frac{\mu 2}{\tan\alpha} \frac{2}{\sqrt{3}} \bar{\sigma} \int_{R_1 - r_0}^{R_0 - r_0} \left[1 - \left(\frac{1+B}{B}\right) \left\{1 - \left(\frac{h}{R_o - r_o}\right)^B\right\}\right] dr \tag{40}$$

which upon simplification is

$$F_2 = 2\pi r_0 \frac{2\bar{\sigma}}{\sqrt{3}} t_1 \left(\frac{\mu 2}{\mu_1 - \mu_2}\right) \left\{1 - \left(\frac{1}{t_o}\right)^B\right\} \tag{41}$$

$$\mu_1 \neq \mu_2$$

If $\mu_1 = \mu_2 = \mu$ then this is modified to read

$$F_2 = 2\pi r_0 \frac{2\bar{\sigma}}{\sqrt{3}} \frac{\mu}{\tan\alpha} t_1 \ln\left(\frac{t_0}{t_1}\right) \tag{42}$$

$$\mu_1 = \mu_2 = \mu$$

The drawing stress is obtained by summing F_1 and F_2 and dividing by the exit area $\pi (R_1^2 - r_0^2)$. Thus the specific draw stress is

$$\sigma_D = \frac{2\bar{\sigma}}{\sqrt{3}} \left(\frac{1+B}{B}\right) \cdot \left[1 - \left(\frac{t_1}{t_0}\right)^B\right] +$$

$$\frac{4}{\sqrt{3}} \bar{\sigma} \frac{r_0}{R_1^2 - r^2} t_1 \left(\frac{\mu 2}{\mu_1 - \mu_2}\right) \left[1 - \left(\frac{t_1}{t_0}\right)^B\right] \qquad (43)$$

$$\mu_2 \neq \mu_1$$

$$\sigma_D = \frac{2\bar{\sigma}}{\sqrt{3}} \left(\frac{1+B}{B}\right) \left[1 - \left(\frac{t_1}{t_0}\right)^B\right] +$$

$$\frac{4\bar{\sigma}}{\sqrt{3}} \left(\frac{\pi r_0}{(R_1^2 - r_o^2)}\right) t_1 \frac{\mu}{\tan\alpha} \ln\left(\frac{t_0}{t_1}\right) \qquad (44)$$

$$\mu_2 = \mu_1 = \mu$$

Equations 43 and 44 are the design equations for potential failure. The failure prediction procedure is as follows:

1. Equation 43 or 44 is evaluated using the appropriate geometric and frictional factors. The value of $\bar{\sigma}$ used must be the tensile yield stress at the exit under whatever temperature and strain rates are experienced by the shell at the exit.

2. For a cold draw at low speeds $\bar{\sigma}$ can be taken as the ordinary sequence of values of $\bar{\epsilon}$ from a stress-strain curve. In this case only work hardening is important; that is

$$\bar{\sigma} = \bar{\sigma}\ (\bar{\epsilon}) \qquad (45)$$

3. For a hot draw at moderate or high speeds, the effects of strain-rate at the temperature of the draw is important; that is

$$\bar{\sigma} = \bar{\sigma}\ (\dot{\bar{\epsilon}}, \bar{\epsilon}) \qquad (46)$$

4. Both cases mentioned above have been automatically covered in one computer program SHELL. In this program Equations 43 and 44 are evaluated using estimates of the effects of strain rate and strain hardening.

III. HEAT TRANSFER

As mentioned previously, the effect of temperature on a drawing process is primarily seen in the influence of strain rate on the lowering of metal strength at elevated speeds and temperatures. As a general conclusion: The higher the mandrel speed (or the higher the strain-rate), the more critical is the operating temperature. As the temperature is raised not only is the metal strength degraded but other physical properties change as well. Among these are the density, specific heat and thermal conductivity. As is well known when these quantities depend on temperature, the net resulting effect on the governing equations in nonlinearity. In addition, since the temperature will vary from point to point in the workpiece so will the various properties and, hence, the conduction of heat. In order to assess this later effect, conductive inhomogeneity, the problem of heat conduction in a nonhomogeneous medium was studied.

Consider the case in the linear theory in which heat transfer diffusion depends upon a single spacial coordinate, x, and time, t. Then the fundamental conservation equation to be solved in the cartesian, cylindrical or spherical coordinate systems is [25, 26]

$$\frac{1}{\bar{x}^m} \frac{\partial}{\partial \bar{x}} \left[\bar{K} \bar{X}^m \frac{\partial \bar{T}}{\partial \bar{x}} = \right] \bar{\rho}\, \bar{c} \frac{\partial \bar{T}}{\partial \bar{t}} \tag{47}$$

where m has the value 0, 1 or 2 according as to whether cartesian, cylindrical or spherical symmetry is being considered. If heat conduction is being considered $\bar{K}$ is the conductivity, $\bar{\rho}$ is the density and $\bar{C}$ the specific heat. If diffusion is being considered, the produce $\bar{\rho}\,\bar{C}$ is unity and $\bar{K}$ is the diffusion constant. $\bar{K}$, $\bar{\rho}$ and $\bar{C}$ are assumed to be specified functions of $\bar{x}$, but independent of $\bar{t}$. In what follows the general form of 1 will be employed.

Consider the initial boundary value problem on $\bar{x}_o \leq \bar{x} < \infty$ for Equation 47. At $\bar{x} = \bar{x}_o$ the temperature is specified

$$\bar{T}\,(x_o,\ 0) = \bar{T}_o\ H\,(\bar{t}), \tag{48}$$

where T_o is an amplitude constant and H $(\bar{t})$ is the Heavyside step function. As $\bar{x} \to \infty$ it is anticipated on physical grounds that

$$\lim_{\bar{x} \to \infty} T\,(\bar{x}, t) = 0 \tag{49}$$

with a similar condition on the flux, $-K\ \partial T/\partial x$. The initial condition is that no heat is transferred prior to $\bar{t} = 0$ or

$$\bar{T}\ (x,\ 0) = 0, \tag{50}$$

At this point it is convenient to introduce dimensionless variables as follows:

$$x = \bar{x}/\bar{x}_o, \qquad \rho = \rho/\rho_o, \qquad t = \bar{t}\ \frac{\bar{K}_o}{\bar{\rho}_o\ \bar{C}_o\ \bar{x}_o^{\,2}}$$

$$T = \bar{T}/\bar{T}_o, \qquad C = \bar{C}/\bar{C}_o, \qquad K = K/K_o, \tag{51}$$

where $\bar{T}_o$, $\bar{C}_o$, ρ_o, $\bar{K}_o$ are the values of the obvious variables at $\bar{x} = \bar{x}_o$. Using Equations 51, 47-49 and 50 become respectively,

$$\frac{\partial}{\partial x}\left[K\ x^m\ \frac{\partial T}{\partial x}\right] = \rho\ C\ \frac{\partial T}{\partial t}\ , \tag{52}$$

$$T\ (1, 0) = H(t), \tag{53}$$

$$\lim_{x \to \infty} T\ (x, t) = 0, \tag{54}$$

and

$$T\ (x, 0) = 0, \tag{55}$$

THE TRANSFORMED PROBLEM

It will now be shown that an equation of the form of Equation 47 is amenable to analytic solution if the following choices for K, ρ , and c are made

$$K = x^{\sigma}, \tag{56}$$

$$\rho = x^{\lambda}, \tag{57}$$

$$c = x^{r}, \tag{58}$$

where σ, q and r are constants. Using Equations 56 to 58, Equation is

$$\frac{\partial}{\partial x}\left[x^{(\sigma + m)}\ \frac{\partial T}{\partial x}\right] - X^s\ \frac{\partial T}{\partial t} = 0, \tag{59}$$

where

$$s = \lambda + r, \tag{60}$$

is introduced for convenience.

Thus, at this point, a solution to Equation 59, subject to Equations 53 to 55 is sought. To this end the Laplace Transform of Equation 59 is taken, which, after the use of Equation 55, is

$$\frac{d}{dx}\left[x^{(\sigma + m)} \frac{d\tilde{T}}{dx}\right] - X^s \; p \; \tilde{T}, \tag{61}$$

In Equation 61 $\tilde{T}$ is the Laplace transform of T and p is the transform parameter defined through

$$\mathcal{L}\,T[(x,t)] \equiv \int_o^\infty e^{-pt} \; T \; dt \quad \tilde{T}\,(x,p), \tag{62}$$

In what follows, the superscript ~ will denote the transform of the obvious quantity.

The boundary conditions, Equations 53 and 54 take the forms, respectively,

$$\tilde{T}\,(1,p) = 1/p, \tag{63}$$

$$\lim_{x \to \infty} \tilde{T}\,(x,p) = 0. \tag{64}$$

It may be recognized, carrying out the indicated differentiation, that Equation 61 is a modified Bessel equation, provided that $S + 2 \neq \sigma$. The general solution to that equation is

$$\tilde{T}\,(x,p) = x^a \left[A(p)\; K_n\left(q\,\frac{x^\beta}{\beta}\right) + B\,(p)\; I_n\left(q\,\frac{x^\beta}{\beta}\right)\right], \tag{65}$$

where

$$\begin{aligned} a &= \left[1 - (m + \sigma)\right]/2, \\ \beta &= \left[S + 2 - \sigma\right]/2, \\ n &= -a/\beta \\ q &= p^{1/2} \end{aligned} \tag{66}$$

The solution which satisfies the boundary condition 63 and the initial conditions, but not necessarily the far field condition, Equation 64, is

$$A(p) = \left[p K_n (q/c) \right]^{-1} \tag{67}$$

$$B(p) = 0 \tag{68}$$

SHORT TIME SOLUTION

Following the method of Reference 26 a solution of Equations 65, 67 and 68 is sought. Omitting the details (which are in Reference 26), Equation 65 is expanded in an asymptotic series

$$\bar{T}(x, p) \sim x^{(a - \beta/2)} \cdot \frac{1}{p} \cdot \exp\left[\frac{-q}{\beta} (x^{\beta} - 1) \right] \cdot \left\{ 1 + c_1/q + c_2/q^2 + \ldots \right\} \tag{69}$$

where

$$c_1 = A_1 - B_1 \tag{70}$$

$$c_2 = A_2 - B_2 - B_1 (A_1 - B_1) \tag{71}$$

and . . .

$$A_1 = \frac{(4n^2 - 1)}{8} \beta x^{-\beta}$$

$$A_2 = \frac{(4n^2 - 1)(4n^2 - 9)}{128} \beta^2 x^{-2\beta}$$

. . . (72)

$$B_1 = \frac{(4n^2 - 1)}{8} \beta$$

$$B_2 = \frac{(4n^2 - 1)(4n^2 - 9)}{128} \beta^2$$

. . .

The inverse of the image function given in 69 may be obtained from standard transform-pair tables. The resulting approximation to T (x, t) is then

$$T(x, t) \sim x^{(a - B/2)} \cdot \left\{ \operatorname{erfc}\left(a/2t^{1/2}\right) + c_1 (4t)^{1/2} \, i \operatorname{erfc}\left(a/2t^{1/2}\right) + c_2 (4t) \, i^2 \operatorname{erfc} \right\} \tag{73}$$

where

$$i^n \text{ erfc } z = \int_z^\infty i^{n-1} \text{ erfc } \xi \, d\xi \qquad n = 1, 2, \ldots \tag{74}$$

are Hartree's repeated complementary error functions.

ACCURATE APPROXIMATE SOLUTION

In order to effect a more accurate solution, the method of Bickford[29] is applied to Equation 65. In this method the functions $K_n(z)$ are presented by

$$K_n(z) \sim \exp(-z) \cdot \left[\pi / 2Z \right]^{1/2} \cdot P_j(z) \tag{75}$$

where

$$P_j(z) = \frac{Z^j + a_1 Z^{j-1} + \ldots a_j}{Z^j + b_1 Z^{j-1} + \ldots b_j} \tag{76}$$

is a rational function of two polynomials of order j. The coefficients are chosen by forcing the right-hand side of Equation 75 to yield exact values for $K_n(z)$ at 2j discrete points. For the present paper adequate accuracy was obtained by choosing j = 1. The values of a_1, b_1 used for this representation are in Table A-3. The result of this calculation gives:

$$\tilde{T} = f_1 p^1 [(q + b_1 \beta x^{-\beta})^{-1} - (q + a_1 \beta)^{-1}] \cdot [p + q f_2 + f_3] \cdot \exp[-q f_4] \tag{77}$$

where

$$\begin{aligned} f_1 &= x^{(z - 1/2)} / [a_1 - b_1 x^{-\beta}] \beta \\ f_2 &= (b_1 + a_1 x^{-\beta}) \beta \\ f_3 &= a_1 b_z \beta^2 x^{-\beta} \\ f_4 &= \frac{1}{\beta} (x^\beta - 1) \end{aligned} \tag{78}$$

The inversion of 77 yields

$$T(x,t) = f_1 f_5 \left\{ \exp[f_6^2 t + f_6 f_4] \cdot \text{erfc}[f_6 t^{1/2} + f_4 / 2t^{1/2}] - \exp[a^2 \beta^2 t + a_1 \beta f_4] \cdot \text{erfc}[a_1 \beta t^{1/2} + f_4 / 2t^{1/2}] \right\} + f_1 f_3 \text{ erfc}[f_4 / 2t^{1/2}] \tag{79}$$

TABLE A-3. VALUES OF a_1, b_1 USED IN BESSEL FUNCTION REPRESENTATION

	a_1	b_1
k_o	0.2772	0.3986
k_1	0.5696	0.2023
$k_{1/4}$	0.3031	0.3949
$k_{1/2}$	1.0	1.0

where, in addition to previously defined symbols

$$f_5 = \beta (b - a) (1 - x^{-\beta})$$
$$f_6 = \beta b x^{-\beta} \qquad (80)$$

In general, the solution given by Equation 77 is approximate, and the nature of that approximation is presented below. However, when $k = 0$ or -1 the solution obtained is exact. The instances of $k = 0$ and -1 correspond to homogeneous ($\sigma = 0$) and $\sigma = 4/3$ cases, respectively. These along with some approximate solutions are shown in Figures A-4 and A-5.

Table A-4 shows the values of $|n|$ and β corresponding to the various values of in $K(x) = x^{\sigma}$ which are used here. Table A-3 shows the values of a_1 and b_1 used in the present study.

TABLE A-4. VALUES OF $|n|$ AND β CORRESPONDING TO VARIOUS σ in $k = x^{\sigma}$.

σ	n	β
0	1/2	1/2
2/3	1/4	2/3
1	0	1/2
4/3	1/2	1/3
3/2	1	1/4

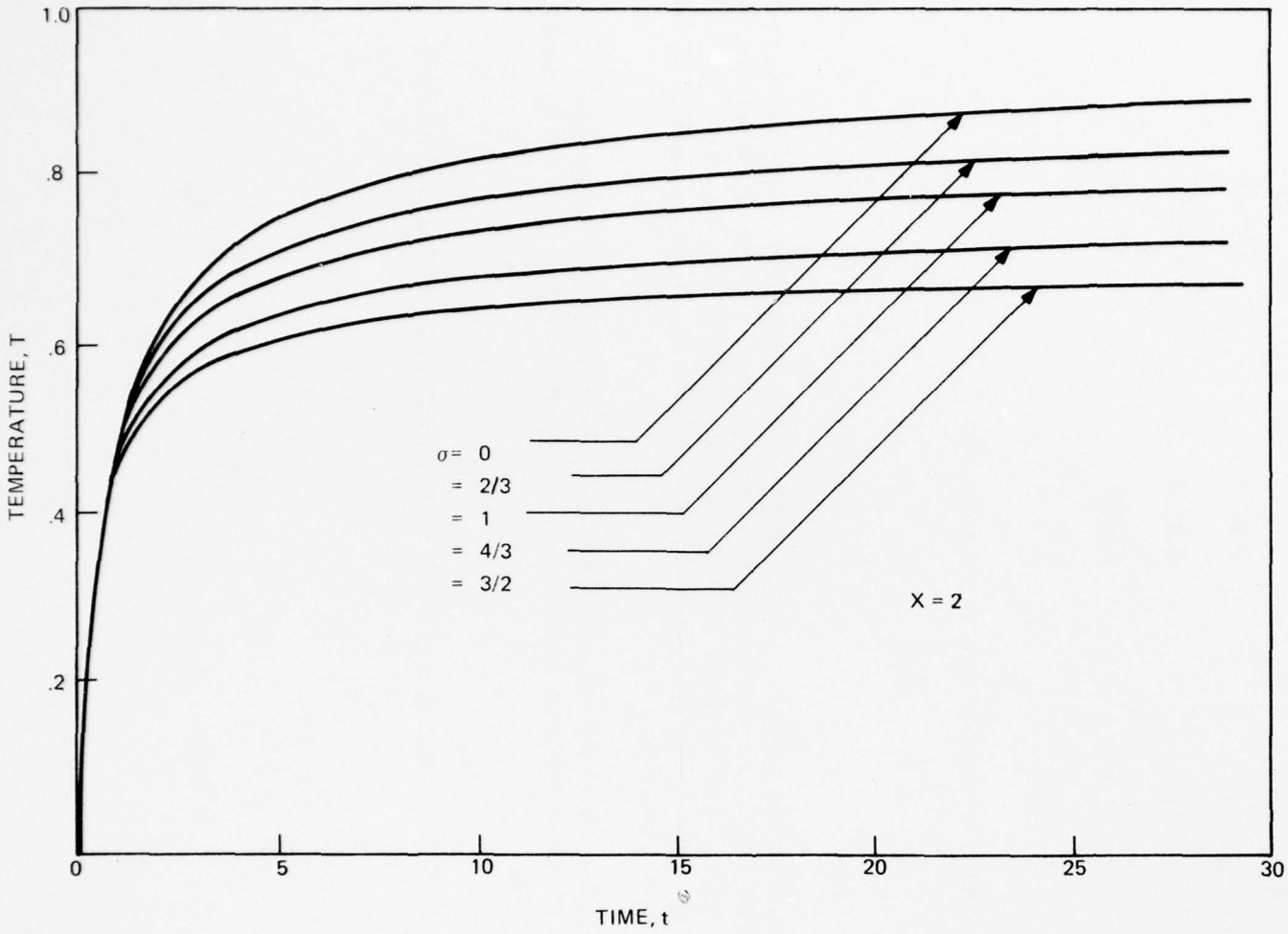

Figure A-4. Temperature vs. Time at x = 2 for Various Values of the Conductivity: $k(x) = x^{\sigma}$.

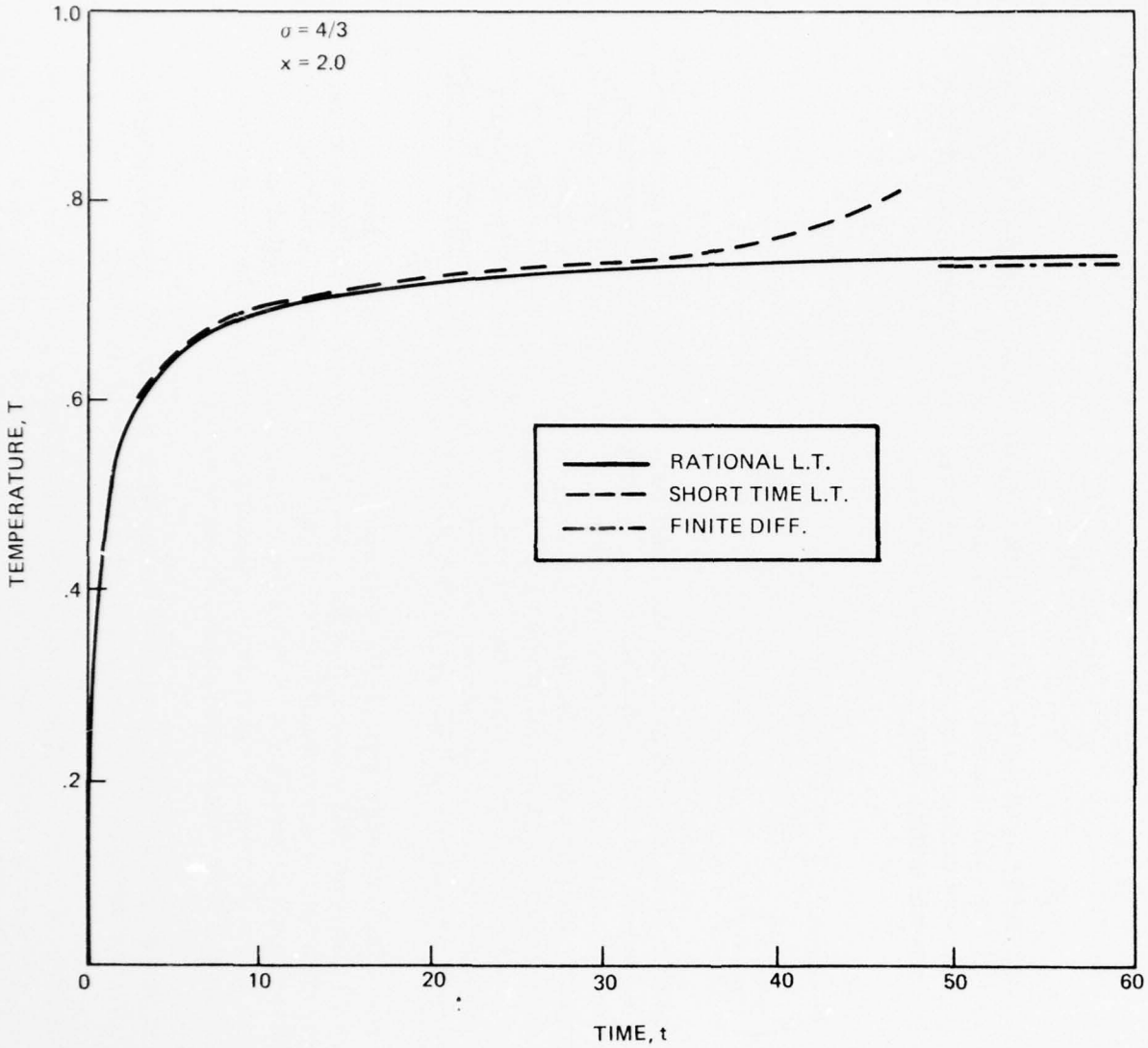

Figure A-5. A Comparison of the Short Time and Rational Polynomial Methods of Solution

Figure A-4 shows the calculation of the temperature, T as a function of time at $x = 2$ for $\sigma = 0,\ 2/3,\ 1,\ 4/3$ and $3/2$ in $k(x) = x^{\sigma}$. At $x = 2$ the value of the conductivity varies from 1 (for $\sigma = 0$) to 2.83 (for $\sigma = 3/2$). However, the temperature difference between the $\sigma = 0$ and $\sigma = 3/2$ curves is on the order of only 25%. Thus, even with a very large difference in conductivity, the resulting temperature difference is not great. It is concluded that, for practical purposes, one should compare heat transfer calculations based on properties evaluated at the extremes of processing variables.

IV FAILURE MODELS

It has been tacitly assumed in this report that failure occurs only when the mandrel punches through the shell, caused by a tensile failure in the shell wall. The criterion for this to occur was defined to be the case at which the specific draw stress or draw stress ratio exceeds unity. Thus it was expressed as

$$\frac{\sigma_f}{\left(\frac{2}{\sqrt{3}}\bar{\sigma}\right)} \geq 1$$

In this equation: σ_f is the tension in the shell wall and σ is the local yield stress in the shell wall beyond the die exit. The tension, σ_f, is found as a result of computation within the model. It is thus a theoretical quantity. The yield strength $\bar{\sigma}$ is determined partly by theory and partly by experiment. As discussed earlier in this report, $\bar{\sigma}$ is a function of temperature, strain and strain rate. The temperature is an assigned quantity. The strain and strain rates are computed within the model. These theoretical quantities are, however, fed into experimental data when used to compute the local yield strength. The details of this were established on page 21.

The above failure model neglects the very real possibility of plastic instability. Reference 30 discusses this concept in detail. Instability in drawing manifests itself by a large, sustained, axial elongation or "necking" of the wall without a corresponding increase in applied drawing load. The point of instability, when plotted on a true stress-true strain diagram, is known to be considerably lower than the ultimate (or fracture) strength of the metal, particularly in hot processing.

One important planned improvement to the model is to have the computer program automatically test the local yield strength, $\bar{\sigma}$, for the point of instability.

On the basis of the above discussion, it is felt that caution must be used in designing dies and processing conditions which result in a specific draw stress close to unity. In such cases it should be determined if the instability limit has already been exceeded.

REFERENCES

1. Lahoti, et al., "Development of a Mathematical Model and Computer Programs Capable of Optimizing the Drawing Process for Actual Artillery Shell and Cartridge Cases", Final Report, Contract DAAA 25-74-C0557 (Army) prepared by Battelle Columbus Labs. Columbus, Ohio, May 1975.

2.a Sachs, G., et al., "Drawing of Thin-Walled Tubing with a Moving Mandrel Through a Single Stationary Die", J. of Appl. Mech., Trans. ASME, 66, 1944, A-199.

2.b Sachs, G., and Epsel, G., "Experimentation on Tube Drawing with a Moving Mandrel", Trans. ASME, 69, 1947, A-81.

3. Hill, R., "The Calculation of Stresses in the Ironing of Metal Cups", J. Iron & Steel Institute, January 1949, p. 41.

4. Green, A. P., "Plane-Strain Theories of Drawing", Proc. of the Inst. Mech. Engrs., London, 174, 1960, 847.

5. Richmond, O., and Devenpeck, M. L., "A Die Profile for Maximum Efficiency in Strip Drawing", Proc. of the 4th U.S. National Congress of Applied Mechanics, Vol. 2, 1962, pp. 1053-57.

6. Devenpeck, M. L., and Richmond, O., "Strip Drawing Experiments with a Sigmoidal Die Profile", Trans. ASME, J. of Engr. for Industry, November 1965, p. 425.

7. Devenpeck, M. L., "Experimental Evaluation of Theoretically Ideal Drawing Dies", p. 215 in Metal Forming - Interrelation Between Theory and Practice, Ed. A. L. Hoffmanner, Plenum Press, 1971.

8. Sowerby, R., et al., "Plane-Strain Drawing and Extrusion of a Rigid-Perfectly Plastic Material Through Concave Dies", Inst. J. Mech. Sciences, 1968, Vol. 10, p. 231.

9. Richmond, O., "Theory of Streamlined Dies for Drawing and Extrusion", in Mechanics of Solide State, edited by F. B. J. Rimrott and J. Schwaighofer, University of Toronto Press, 1968.

10. Hill, R., "Mathematical Theory of Plasticity", London, 1950.

11. Avitzur, "Analysis of Central Bursting Defects in Extrusion and Wire Drawing", ASME Trans., Series B, Vol. 90, No. 1, January 1968, p. 72.

12. DePierre, V., "Mathematical Analyses of Forces in Extrusion and Drawing of Tubes Through Conical Dies with a Moving Cylindrical Mandrel", Tech. Report AFML-TR-69-197, October 1969.

13. Chen, C. T., and F. F. Ling, "Upper-Bound Solutions to Axisymmetric Extrusion Problems", Inst. J. Mech. Sciences, 1968, Vol. 10, p. 863.

14. Chang, K. T. and Choi, J. C., "Upper-Bound Solutions to Tube Extrusion Problems Through Curved Dies", ASME Paper 71-WA/Prod-8.

15. Mehta, H. S., et al., "Analysis of Tube Extrusion", ASME Trans. Journal of Engineering for Industry, May 1970, p. 430.

16. Bishop, J.F.W., "An Approximate Method for Determining the Temperatures Reached in Steady State Motion Problems of Plane Plastic Strain", Quarterly J. of Mech. and Appl. Math Vol. 9, 1956, p. 236.

17. Altan, T., and Kobayashi, S., "A Numerical Method for Estimating Temperature Distributions in Extrusion Through Conical Dies", ASME Trans., J. Engr. Industry, 90, 1968, p. 107.

18. Altan, T., et al., "Approximate Calculation of Velocity and Temperature Distributions in Axisymmetric Extrusion and Drawing", Proceedings of the North American Metalworking Research Conference, May 14-15, 1973, Hamilton, Ontario, Canda, p. 107.

19. Altan, T., "Heat Generation and Temperatures in Wire and Rod Drawing", Wire Journal, March 1970, p. 54.

20. Lahoti, G., and Altan, T., "Prediction of Temperature Distributions in Tube Extrusion Using a Velocity Field without Discontinuities", paper submitted to North American Metalworking Research Conference-II, Madison, Wisconsin, May 20-22, 1974.

21. Lin, C. C., "On a Perturbation Theory Based on the Method Characteristics", Journal of Mathematics and Physics, Vol. 33, 1951, pp. 117-134.

22. Fox, P. A., "Perturbation Theory of Wave Propagation, Vol. 34, 1955, pp. 133-151.

23. Richmond, O., and Morrison, H. L., Journal of Applied Mechanics", March 1968, pp. 117-122.

24. Onat, E. T., "The Effects of Nonhomogeneity Caused Strain Hardening on the Small Deformations of a Rigid-Plastic Solid", Nonhomogeneity in Elasticity and Plasticity, Pergamon, New York, 1959, pp. 171-180.

25. B. Boley and J. Weiner, Theory of Thermal Stresses, New York: John Wiley, 1966.

26. H. Carslaw and J. Jaegar, Conduction of Heat in Solids, 2nd ed., Oxford, England: Oxford U. Press, 1959.

27. G. N. Watson, A Treatise on the Theory of Bessel Functions, Cambridge Univ. Press, 1948, New York, 2nd ed., p. 80.

28. W. B. Bickford, "A Note on Rational Approximations of Transcendental International Textbook Co., 1968, pp. 301-343.

29. Altan, T. and Boulger, F. W., Trans. ASME, J. Engr. for Industry, Vol. 95, Nov. 1975, pp. 1009-1019.

30. Marin, J., Engineering Materials, Prentice-Hall, 1952, NY, pg. 53-57.

DISTRIBUTION

Commander
US Army Materiel Development &
Readiness Command
5001 Eisenhower Avenue
Alexandria, VA 22333

1 Attn: DRCDMD

1 Attn: DRCDMR

1 Attn: DRCDMD-T

1 Attn: DRCD-L,
Foreign Science &
Technology Division

1 Attn: DRCDE-E,
Edson Gardner

1 Attn: DRCDE-W

1 Attn: DRCDE-W

1 Attn: DRCMT,
L. Croan

1 Attn: DRCMT,
Col. N. Vinson

1 Attn: DRCDE-DE,
E. Lippi

Commander
Rock Island Arsenal
Rock Island, IL 61202

1 Attn: Technical Information Div.

1 Attn: SARRI-R

Commander
Aberdeen Proving Ground
Attn: STEAP-TL, Technical Library
Aberdeen, MD 21005

Commander
US Army Harry Diamond Laboratories
2800 Powder Mill Road
Attn: AMXDO-TIB
Adelphia, MD 20783

Commander
US Army Armament Command
Rock Island, IL 61201

1 Attn: Technical Information Div.

1 Attn: DRSAR-PPI-W,
A. Zahatko

1 Attn: DRSAR-RD,
Mr. J. Brinkman

1 Attn: DRSAR-RDG-A,
Mr. J. Williams

1 Attn: PM, CAWS,
Mr. H. Noble

Commander
US Army Materials & Mechanics
Research Center
Watertown, MA 02171

1 Attn: DMXMR,
Dr. E. Wright

1 Attn: Technical Information Div.

Commander
Picatinny Arsenal
Dover, NJ 07801

1 Attn: PM,
Selected Ammunition

1 Attn: SARPA-FR-M,
Chf, Materials Eng. Div.

1 Attn: SARPA-AD

1 Attn: SARPA-AD-D-A-3,
M. Margolin

1 Attn: DRCPM-PBM-M,
H. Krasser

1 Attn: DRCPM-PBM-M,
M. Kolisek

1 Attn: Technical Information Div.

1 Attn: SARPA-MT

DISTRIBUTION (Cont)

Commander
Watervliet Arsenal
Watervliet, NY 12189

1 Attn: SARWV-RD

1 Attn: SARWV-RDR,
Dr. E.E. Davidson

1 Attn: Technical Information Div.

Commander
US Army Research Office
P.O. Box 12211
Attn: Dr. George Mayer, Director
Metallurgy & Materials
Science Division
Research Triangle Park, NC 27709

Commander
Naval Air Development Center
Johnsville, Aero Materials Dept.
Attn: Mr. Forrest Williams
Warminister, PA 18974

Commander
US Army Natick Research & Development Command
Attn: Technical Information Div.
Natick, MA 07160

Commander
Naval Air Systems Command
Department of the Navy
Attn: AIR 5203, Mr. R. Schmidt
Washington, DC 20361

Commander
Naval Ships Systems Command
Department of the Navy
Attn: Code 03423
Washington, DC 20025

Commander
Office of Naval Research
Department of the Navy
Attn: Code 423
Washington, DC 20023

Commander
US Army Foreign Science & Technology Center
Attn: Mr. William F. Marley
220 7th Street N.E.
Charlottesville, VA 22901

Commander
US Naval Weapons Laboratory
Attn: Technical Information Div.
Dahlgren, VA 22448

Commander
US Naval Engineering Experimental Station
Attn: WCTRL-2, Materials Lab.
Annapolis, MD 21402

Commander
Air Research & Development Command
Andrews Air Force Base
Attn: RDRAA
Washington, DC 20025

Commander
US Naval Ordnance Laboratory
Attn: Code WM
Silver Spring, MD 20910

Commander
Aeronautical Systems Division
Wright-Patterson Air Force Base
Attn: Technical Information Div.
Dayton, OH 45433

Commander
Rep, Alabama Army Ammunition Plant
Childersburg, AL 35044

DISTRIBUTION (Cont)

Commander
Rep, Badger Army Ammunition Plant
Baraboo, WI 53919

Commander
Rep, Burlington Army Ammunition Plant
Burlington, NJ 08016

Commander
Rep, Cornhusker Army Ammunition Plant
Grand Island, NB 68801

Commander
Rep, Gateway Army Ammunition Plant
St. Louis, MO 63143

Commander
Rep, Hays Army Ammunition Plant
Pittsburgh, PA 15207

Commander
Holston Army Ammunition Plant
Kingsport, TN 37622

Commander
Indiana Army Ammunition Plant
Charlestown, IN 47111

Commander
Iowa Army Ammunition Plant
Middletown, IA 52638

Commander
Rep, Joliet Army Ammunition Plant
Joliet, IL 60436

Commander
Kansas Army Ammunition Plant
Parsons, KS 67357

Commander
Lake City Army Ammunition Plant
Independence, MO 64050

Commander
Lone Star Army Ammunition Plant,
Texarkana, TX 75502

Commander
Longhorn Army Ammunition Plant
Marshall, TX 75671

Commander
Louisiana Army Ammunition Plant
Shreveport, LA 71130

Commander
Milan Army Ammunition Plant
Milan, TN 38358

Commander
Newport Army Ammunition Plant
Newport, IN 47966

Commander
Radford Army Ammunition Plant
Radford, VA 24141

Commander
Rep, Ravenna Army Ammunition Plant
Ravenna, OH 44266

Commander
Riverbank Army Ammunition Plant
Riverbank, CA 95367

Commander
Scranton Army Ammunition Plant
Scranton, PA 18501

Commander
Rep, St. Louis Army Ammunition Plant
St. Louis, MO 63160

Commander
Rep, Sunflower Army Ammunition Plant
Lawrence, KS 66044

Commander
Twin Cities Army Ammunition Plant
New Brighton, MN 55112

Commander
Volunteer Army Ammunition Plant
Chattanooga, TN 37401

DISTRIBUTION (Cont)

Commander
Edgewood Arsenal
Attn: SAREA-MT
Aberdeen Proving Ground, MD 21010

US Army Mobility Equipment
Research & Development Command
Attn: STSFB-MMM, Mr. W. Baer
Ft. Belvoir, VA 22060

Commander
Redstone Arsenal
Attn: Technical Information Div.
Huntsville, AL 35809

Commander
Rocky Mountain Arsenal
Attn: Technical Information Div.
Denver, CO 80240

Director
Air Force Materials Laboratory
Attn: AFML, Technical Library
Wright-Patterson AFB
Dayton, OH 45433

Director
National Academy of Science
Attn: Materials Advisory Board
2101 Constitution Avenue, N.W.
Washington, DC 20418

Metals & Ceramic Information Center
Battelle Memorial Institute
505 King Avenue
Columbus, OH 43201

Director
US Army Air Mobility Research &
Development Center
Ames Research Center
Attn: Mr. Paul Yaggy
Moffet Field, CA 94035

Director
US Army Production Equipment Agency
Attn: DRXPE, J. Gallaugher
Rock Island, IL 61201

Director
US Army Advanced Materials Concept
Agency
Attn: Technical Information Div.
2461 Eisenhower Avenue
Alexandria, VA 22314

Director
US Naval Research Laboratory
Attn: Mr. W.S. Pellini, Code 6300,
Metallurgy Div.
Washington, DC 20390

Director
Naval Ships Research & Development
Center
Attn: Mr. Abner R. Willmer,
Chief of Metals Research
Bethesda, MD 20034

Director
Air Force Armament Laboratory
Attn: AFATL/DLOSL
Eglin AFB, FL 32542

Director
Air Force Weapons Laboratory
Attn: Technical Information Div.
Kirtland AFB. NM 87118

Director
Air Force Materials Laboratory
Wright-Patterson Air Force Base
Dayton, OH 45433

1 Attn: AFML/LLD,
Dr. T.M.F. Ronald

1 Attn: AFML,
Technical Library

Director
Defense Advanced Research Projects
Agency
Attn: Dr. E.C. Van Reuth
1400 Wilson Boulevard
Arlington, VA 22209

DISTRIBUTION (Cont)

Director
National Academy of Science
Attn: Materials Advisory Board
2101 Constitution Avenue, N.W.
Washington, DC 20418

Director
National Aeronautics & Space Administration
Attn: Code RPM
Federal Building #10
Washington, DC 20546

Director
National Bureau of Standards
Attn: Technical Information Div.
Washington, DC 20025

FederalAviation Administration
Attn: Administrative Standard Div.
800 Independence Avenue, S.W.
Washington, DC 20690

Chief
Bureau of Ships
Department of the Navy
Attn: Code 343
Washington, DC

Chief
Bureau of Aeronautics
Department of the Navy
Attn: Technical Information Div.
Washington, DC

Chief
Bureau of Weapons
Department of the Navy
Attn: Technical Information Div.
Washington, DC

US Atomic Energy Commission
Document Library
Germantown, MD 21403

Mr. Robert H. Brown
1411 Pacific Avenue
Natrona Heights, PA 15065

Dr. Robert S. Busk
3606 Windsor Court
Midland, MI 48640

Mr. J.B. Hess
Kaiser Aluminum & Chemical Corp.
Aluminum Division Research Center for Technology
P.O. Box 870
Pleasanton, CA 94566

Dr. Schrade Radtke
International Lead Zinc Institute
292 Madison Avenue
New York, NY 10017

Prof. M.C. Flemings
Department of Metallurgy
Materials Science
Mass. Institute of Technology
Cambridge, MA 02139

Mr. Carson L. Brooks
Reynolds Metal Company
4th & Canal Streets
Richmond, VA

Mr. Harold Hunsicker
Aluminum Company of America
Alcoa Technical Center
Alcoa Center, PA 15069

Dr. E.J. Ripling
Materials Research Laboratory, Inc.
1 Science Road
Glenwood, IL 60425

Dr. Thomas E. Leontis
Battelle, Columbus Laboratories
505 King Avenue
Columbus, OH 43201

Defense Documentation Center (12)
Cameron Station
Alexandria, VA 22314

DISTRIBUTION (Cont)

Commander
Frankford Arsenal
Philadelphia, PA 19137

1 Attn: AOA-M

1 Attn: TD

1 Attn: CE

1 Attn: QAA-R

1 Attn: PA

1 Attn: GC

1 Attn: PD

1 Attn: PDM,
R.P. Stanton

1 Attn: PDM,
R.S. Schlauch

1 Attn: PDM,
I.G. Betz

3 Attn: PDM,
Mr. J.D. Corrie

1 Attn: PDM,
H.J. Addison, Jr.

1 Attn: PDM-P

10 Attn: PDM-E,
Mr. P. Gordon

10 Attn: PDM-E,
Mr. F. Lee

1 Attn: PDM-E,
Project File

1 Attn: PDM-A

1 Attn: PDR,
Mr. H. Kahn

Frankford Arsenal (Cont)

1 Attn: MD

1 Attn: MDA,
J. Sikra

1 Attn: MDA-D

1 Attn: MDA-D,
Mr. K. Ryan

1 Attn: MDA-D,
Mr. D. Lenton

1 Attn: MDA-D,
Mr. K. Pitko

1 Attn: MDC,
L. Destefano

1 Attn: MDC,
W. Gadomski

1 Attn: MDC,
B. Siegel

1 Attn: MDC-A,
Mr. F. Shinaly

1 Attn: MDE,
A. Cianciosi

1 Attn: MDM

1 Attn: MDS

1 Attn: MDS-S

1 Attn: FI

1 Attn: MT

2 Attn: MT,
E. Kelley

1 Attn: MT,
H. Huff

DISTRIBUTION (Cont)

Frankford Arsenal (Cont)

3 Attn: MT,
R. Coyle

1 Attn: MTT

3 Attn: TSP-L,
1 - Reference Copy
1 - Circulation Copy
1 - Technical Reports
Editing

Printing & Reproduction Division
FRANKFORD ARSENAL
Date Printed: 14 March 1977

AD-A038 496 FRANKFORD ARSENAL PHILADELPHIA PA F/G 19/1
COMPUTER-AIDED MODELING OF ARTILLERY SHELL AND CARTRIDGE CASE D--ETC(U)
APR 76 P F GORDON, F M LEE
UNCLASSIFIED FA-TR-76020 NL

2 OF 2
AD A038 496

END
DATE FILMED
10-77
DDC

SUPPLEMENTARY

INFORMATION

DEPARTMENT OF THE ARMY
U. S. ARMY ARMAMENT RESEARCH AND DEVELOPMENT COMMAND
DOVER, NEW JERSEY 07801

25 July 1977

ERRATUM SHEET FOR FA REPORT TR-76020 (April 1976)

TITLE: Computer-Aided Modeling of Artillery Shell and Cartridge Case Drawing

AUTHORS: P. F. Gordon and F. M. Lee

1. An error has been discovered in the theoretical formulation and computer solution for the analysis which is given in Appendix A, Section III on pages 68 to 76 of the subject report. As a result the statement: "Thus, even with a very large difference in conductivity, the resulting temperature difference is not great", which appears at the top of page 76, is invalidated. It is further advised that Appendix A - Section III be deleted in order to avoid any possible misuse.

2. The latter finding, however, in no way invalidates the summary and conclusions of those portions of the report pertaining directly to artillery projectiles (pages 43-46).